AGU PUBLICATIONS

JGR

Journal of Geophysical Research: Oceans

RESEARCH ARTICLE

10.1002/2014JC010272

Key Points:
- First direct estimation of nitrate fluxes in the Lower St. Lawrence Estuary
- Fluxes reported are among the highest found in the world ocean
- Fluxes sustain high primary productivity throughout the summer

Correspondence to:
F. Cyr,
frederic.cyr@nioz.nl

Citation:
Cyr, F., D. Bourgault, P. S. Galbraith, and M. Gosselin (2015), Turbulent nitrate fluxes in the Lower St. Lawrence Estuary, Canada, *J. Geophys. Res. Oceans*, *120*, 2308–2330, doi:10.1002/2014JC010272.

Received 4 JUL 2014
Accepted 24 FEB 2015
Accepted article online 26 FEB 2015
Published online 27 MAR 2015
Corrected 13 APR 2015

This article was corrected on 13 APR 2015. See the end of the full text for details.

Turbulent nitrate fluxes in the Lower St. Lawrence Estuary, Canada

Frédéric Cyr[1,2], Daniel Bourgault[1], Peter S. Galbraith[3], and Michel Gosselin[1]

[1]Institut des sciences de la mer de Rimouski, Université du Québec à Rimouski, Rimouski, Québec, Canada, [2]Now at Royal Netherlands Institute for Sea Research, Den Burg, Netherlands, [3]Ocean and Environmental Science Branch, Department of Fisheries and Oceans Canada, Maurice Lamontagne Institute, Mont-Joli, Québec, Canada

Abstract Turbulent vertical nitrate fluxes were calculated using new turbulent microstructure observations in the Lower St. Lawrence Estuary (LSLE), Canada. Two stations were compared: the head of the Laurentian Channel (HLC), where intense mixing occurs on the shallow sill that marks the upstream limit of the LSLE, and another station located about 100 km downstream (St. 23), more representative of the LSLE mean mixing conditions. Mean turbulent diffusivities and nitrate fluxes at the base of the surface layer for both stations were, respectively (with 95% confidence intervals): $\bar{K}_{HLC} = 8.6(3.2, 19) \times 10^{-3}\ m^2\ s^{-1}$, $\bar{K}_{23} = 4.4(2.3, 7.6) \times 10^{-5}\ m^2\ s^{-1}$, $\bar{F}_{HLC} = 95(18, 300)\ mmol\ m^{-2}\ d^{-1}$, and $\bar{F}_{23} = 0.21(0.12, 0.33)\ mmol\ m^{-2}\ d^{-1}$. Observations suggest that the interplay between large isopleth heaving near the sill and strong turbulence is the key mechanism to sustain such high turbulent nitrate fluxes at the HLC (two to three orders of magnitude higher than those at Station 23). Calculations also suggest that nitrate fluxes at the HLC alone can sustain primary production rates of $3.4(0.6, 11)\ g\ C\ m^{-2}\ mo^{-1}$ over the *whole* LSLE, approximately enough to account for a large part of the phytoplankton bloom and for most of the postbloom production. Surfacing nitrates are also believed to be consumed within the LSLE, not leaving much to be exported to the rest of the Gulf of St. Lawrence.

1. Introduction

Nutrient cycling in the global ocean controls the primary production through nutrients availability in the euphotic zone. By fixing atmospheric carbon during photosynthesis, phytoplankton growth also plays an important role in regulating anthropogenic CO_2 concentrations in the atmosphere [e.g., *Tsunogai et al.*, 1999; *Thomas et al.*, 2004; *Arrigo*, 2005]. Nutrient and carbon cycles are therefore closely related and their understanding is crucial for modeling Earth's future climate.

The coastal oceans play a key role in the dynamics of these cycles because they act as buffering zones between the continents, from where they receive large amounts of nutrients and organic matter from land drainage, and the deep ocean, with which they exchange nutrients, particles, and energy. Because of this buffering effect, they are among the most physically and biogeochemically active regions of the oceans [*Gattuso et al.*, 1998; *Borges*, 2005]. Although they occupy a small fraction of the ocean surface (~7%), they sustain about 15–30% of the primary production and contribute to 20–50% of the carbon sequestration in the oceans [*Wollast*, 1998; *Tsunogai et al.*, 1999; *Thomas et al.*, 2004; *Muller-Karger*, 2005]. Large tidally induced turbulent mixing that typically characterizes coastal zones directly affects the magnitude of the oceanic carbon uptake, because primary production sustained by turbulent diapycnal nutrient fluxes is much more efficient for sequestrating carbon than the regenerated production resulting from nutrient recycling [*Falkowski*, 2000; *Richardson et al.*, 2000; *Sharples et al.*, 2001a; *Allen et al.*, 2004; *Rippeth*, 2005; *Rippeth et al.*, 2009]. The aim of this study is thus to explore turbulent diapycnal nutrient fluxes in a region of the world where strong turbulence is believed to sustain high (nearly as high as spring bloom level) primary production rates throughout summer: the Lower St. Lawrence Estuary (LSLE), generally considered part of the Gulf of St. Lawrence (GSL), Canada (Figure 1).

The Gulf of St. Lawrence (Figure 1, inset) is a deep and stratified coastal sea with areas of strong tidally induced turbulence and/or upwellings, as well as large freshwater inputs. The LSLE is deep in that its typical depth (>300 m) is much greater than the thicknesses of surface and bottom boundary layers (~10 m)

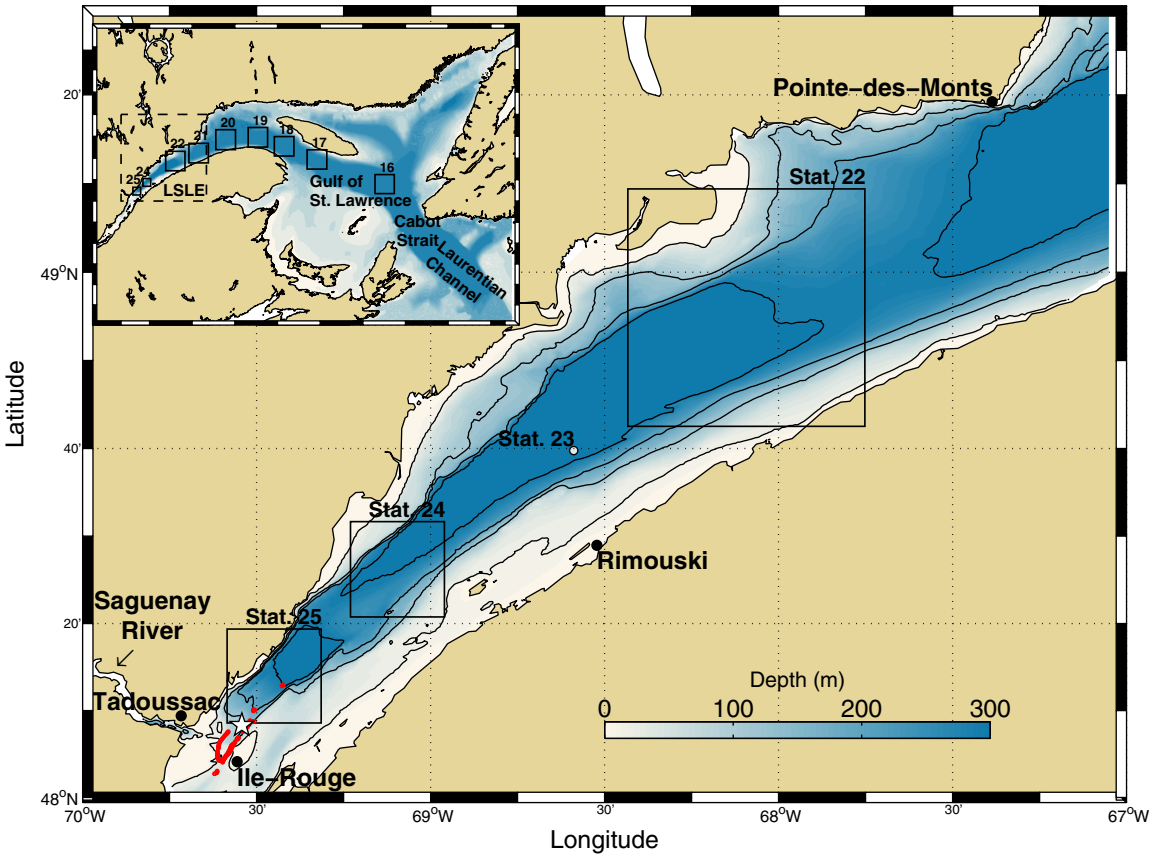

Figure 1. Map and bathymetry of the Gulf of St. Lawrence (inset) and the Lower St. Lawrence Estuary (main plot). Sampling boxes for Stations 16–22, and Stations 24 and 25 have 50 × 50 and 20 × 20 km^2, respectively. Location of monitoring Station 23 is also shown. The fixed station occupied twice in September 2012 is represented by a white star. Sites of the turbulence profiles from the 2009 survey are identified with red dots.

[*Bourgault et al.*, 2012]. According to *Egbert and Ray* [2000], the GSL and the Bay of Fundy basins together occupy the 10th rank among the world coastal seas and shelves for their tidal dissipation level. The GSL is also a biologically rich area hosting many commercially important fish and crustacean species. With landings of about 3–4 × 10^5 metric ton (t) a year, it sustained about 20% of the eastern Canadian fisheries prior to the mid-90s ground fish decline [*Chadwick and Sinclair*, 1991; *de Lafontaine et al.*, 1991]. Historical research on nutrient dynamics and primary and secondary production has thus been considerable in the GSL, although some important processes are still not fully understood such as the nutrient supply to the system by turbulent mixing and upwelling.

The surface nutrient distribution was studied during the *International Biological Program* [*Steven*, 1971, 1974]. A major result of this program was that nutrient supply to the euphotic zone of the GSL was coming from upwelling within the LSLE (Figure 1, main plot), a large-scale estuary (the width is many times the internal Rossby radius) located upstream of the GSL. The nutrient supply to the GSL by the LSLE was referred by *Steven* [1971] as the *nutrient pump*. Further studies suggested that within the LSLE, most of the nutrient surfacing from deeper layers occurs at a localized area at the head of the Laurentian Channel (HLC) near Tadoussac [*Ingram*, 1975; *Greisman and Ingram*, 1977; *Ingram*, 1979a, 1983].

The Laurentian Channel is a long (>1000 km) and deep (>290 m) submarine valley that originates on the continental slope, runs across the Gulf and ends near Tadoussac where the total depth abruptly shallows from 325 m to about 50 m in less than 15 km (Figure 1). It is also where the Saguenay Fjord connects and exchange waters with the LSLE. It has been suggested that intense vertical mixing occurs at this sill, but direct measurements of turbulence have never been collected.

Three water layers are present in the LSLE/GSL system and these circulate with an estuarine-like dynamics affected by rotation along the Laurentian Channel [e.g., *Koutitonsky and Bugden*, 1991;

Saucier and Chassé, 2000; *Saucier et al*., 2009]. The surface layer (upper 30–50 m) is generally fresher in the LSLE compared to the GSL because of high freshwater input from the St. Lawrence and Saguenay rivers. Freshwater inputs also drive the Gaspé Current, a strong surface coastal jet current that contributes to most of the LSLE output to the Gulf [*Tang*, 1980; *Benoit et al*., 1985; *Koutitonsky and Bugden*, 1991]. The bottom layer (roughly below 150–200 m) is composed of salty nutrient-rich waters of Atlantic origin. In between is found the cold intermediate layer (CIL), a remnant of the previous winter Gulf surface layer that was trapped under the warmer/fresher surface waters at the onset of spring [*Banks*, 1966; *El-Sabh*, 1979; *Koutitonsky and Bugden*, 1991; *Gilbert and Pettigrew*, 1997; *Galbraith*, 2006; *Smith et al*., 2006]. Waters below the CIL temperature minimum, which lies roughly at a depth of 60–100 m, have high and almost constant nutrient concentrations [*Steven*, 1974]. The vertical exchanges between the nutrient-rich layer and the surface layer are however generally low, because of the weak turbulent ventilation that is also responsible for hypoxic conditions in the deep LSLE [*Gilbert et al*., 2005; *Bourgault et al*., 2012].

While spring blooms that occur in the Gulf leaves the surface layer generally nutrient-depleted, the nutrient concentrations in the LSLE surface waters remain high [*Steven*, 1971, 1974]. This is because both the intermediate and the bottom layers are thought to be partly upwelled and vertically mixed at the HLC [*Ingram*, 1979a, 1983; *Saucier et al*., 2009]. About 75% of the surface nutrients found in the LSLE may therefore originate from the CIL because of this upwelling/mixing mechanism [*Greisman and Ingram*, 1977; *Savenkoff et al*., 2001], the remaining part being attributed to the St. Lawrence and Saguenay rivers discharge. These vertical nutrient fluxes at the HLC sustain a high primary productivity in the LSLE, with daily production rates during the summer nearly equivalent to those during spring blooms [*Levasseur et al*., 1984; *Therriault and Levasseur*, 1985; *Plourde and Runge*, 1993; *Plourde et al*., 2001]. This high primary productivity sustains high levels of secondary production that is then exported to the Gulf, mostly via the Gaspé Current [*Fortier et al*., 1992; *Plourde and Runge*, 1993]. Recently, *Ouellet et al*. [2013] also suggested that the LSLE has an important role for the development and growth of the GSL capelin population, which itself is important for biomass transfer to upper trophic levels. Nutrient pumping at the HLC is thus likely a keystone for food web dynamics, not only for the LSLE but also for the Gulf.

In contrast to previous studies which indirectly inferred vertical nutrient fluxes at the HLC [*Greisman and Ingram*, 1977; *Savenkoff et al*., 2001], this study presents direct measurements of turbulence profiles from which vertical nutrient fluxes are derived. The study focuses mainly on nitrate fluxes since dissolved nitrogen is thought to be the limiting nutrient in the system [*Steven*, 1974; *Levasseur and Therriault*, 1987]. Comparison will also be made between observed mixing and fluxes at the HLC and at another station located about 100 km downstream.

2. Methodology

2.1. Nutrient Concentration Data

Nutrient concentrations were obtained from the Ocean Data Management System public database [*Fisheries and Oceans—Canada*, 2013]. All water bottle measurements of $NO_3 + NO_2$ (nitrate plus nitrite) concentrations available for the period 2000–2012 and between April and November are considered. These measurements are also accompanied with other physical measurements such as temperature and salinity. Except for Station 23, these measurements are located within a square box roughly the width of the Laurentian Channel and centered on oceanographic stations 16–25 (Figure 1). These stations were selected since they have been routinely visited for multidisciplinary studies in the GSL [e.g., *Benoit et al*., 2006; *Lehmann et al*., 2009]. Since Station 23 has been visited quasi-weekly from May to November by scientists from the Maurice Lamontagne Institute as part of a monitoring program (actual *Station Rimouski* in the Atlantic Zone Monitoring Program [*Plourde et al*., 2008; *Galbraith et al*., 2014]), these measurements were selected. All other measurements were grouped per station. This method is similar to that of *Bourgault et al*. [2012], except a box of 20×20 km^2 is considered here for Station 25 instead of 10×10 km^2. On average, 54 profiles were extracted per station. Station 23 contains the highest number of casts ($n = 254$), while Station 24 contains the least number ($n = 7$).

Since $NO_3 + NO_2$ concentration measurements are from various investigators, different methods were used [*Clesceri et al*., 1989; *Grasshoff et al*., 1999; *Mitchell et al*., 2002]. To the best of our knowledge, they were all

measured with autoanalyzers, whether of type Alpkem, Technicon II, or Bran-Luebbe 3. For the remainder of the article, we will refer to $NO_3 + NO_2$ concentrations as *nitrate* concentration. This approximation is justified since for more than 95% of the water samples, NO_2 concentration represents less than 7% of the total $NO_3 + NO_2$ concentration.

Another survey conducted 13 h sampling, i.e., covering the semidiurnal tidal period, on both 23 and 29 September 2012 from the R/V Coriolis II in proximity to Station 25 (see white star in Figure 1). During station occupation, conductivity-temperature-depth (CTD) casts were conducted nearly every hour with a Sea-Bird SBE 9. Every 3 h, Niskin bottle samples were taken for nutrient concentration analyses. An echo sounder (Simrad EK-60) and a 150 kHz Acoustic Doppler Current Profiler (RDI-ADCP) were also sampling the water column during this survey.

2.2. Turbulence Data

Turbulence measurements were collected with a free falling, loosely tethered Vertical Microstructure Profiler (VMP500) from Rockland Scientific International (RSI), deployed from a small boat. This profiler is equipped with Sea-Bird Electronic sensors for fine scale ($\sim 10^{-1}$ m) measurements of pressure, temperature T, and practical salinity. Salinity measurements presented in this study have been converted to absolute salinity S_A (g kg^{-1}) [*McDougall and Barker*, 2011]. Along with other microscale ($\sim 10^{-2}$ m) sensors, the VMP is equipped with two airfoil shear probes (SPM-38 from RSI) that allow measurements of the microscale vertical shear $\left(\frac{\partial u'}{\partial z}\right)$.

A total of 817 turbulence profiles were collected at Station 23 during summers 2009–2012. Most have already been used in two previous studies [*Cyr et al.*, 2011; *Bourgault et al.*, 2012]. As they were collected from a small boat, they were conducted in relatively calm sea conditions. The maximum depth of VMP casts at this station varied between 180 and 325 m (bottom depth).

Our team also collected 207 turbulence profiles at the HLC near Station 25 between 29 September 2009 and 2 October 2009 (red dots in Figure 1), a period corresponding to a neap-tide phase of the fortnightly tide cycle (smallest high tide on 27 September). To avoid snagging the profiler on the rocky bottom, profiles at the HLC were performed as close as possible to the seabed (our target was to reach within 2–5 m of the seabed) without intentionally hitting it. These observations were also carried out under relatively calm sea conditions (the wind generally did not exceed 20 km h^{-1} except for 30 September where it reached 40 km h^{-1} for an hour at the nearest meteorological station on *Ile Rouge*). During the VMP sampling at the HLC, a 600 kHz RDI-ADCP was deployed on the side of the boat at a depth of about 1 m below the surface. The vertical resolution was 0.5 m and ensembles of 35 pings were averaged every 10 s. This allowed current measurements (U, V) from which the vertical shear ($S^2 = \overline{\left(\frac{\partial U}{\partial z}\right)^2} + \overline{\left(\frac{\partial V}{\partial z}\right)^2}$, in s^{-2}) was calculated.

Turbulence data reduction for both stations was achieved using a procedure similar to that described in previous studies in the LSLE [e.g., *Cyr et al.*, 2011; *Bourgault et al.*, 2012] and briefly summarized here. Dissipation rates of turbulent kinetic energy (ϵ, in W kg^{-1}) were calculated by [e.g., *Lueck et al.*, 2002; *Sundfjord et al.*, 2007; *Rippeth et al.*, 2009; *Martin et al.*, 2010]:

$$\epsilon = \frac{15\nu}{2}\overline{\left(\frac{\partial u'}{\partial z}\right)^2}, \tag{1}$$

where $\nu = f(T)$ is the kinematic molecular viscosity (in m^2 s^{-1}) as a function of temperature and the overline indicates here a vertical 1 m bin averages. The shear variance $\overline{\left(\frac{\partial u'}{\partial z}\right)^2}$ was obtained by spectral integration with care taken to exclude, when necessary, high wave number instrumental noise.

Turbulent diffusivities (K, in m^2 s^{-1}) were calculated from the dissipation rates as:

$$K = \frac{\Gamma\epsilon}{N^2}. \tag{2}$$

Here $N^2 = -\frac{g}{\rho}\frac{\partial \rho}{\partial z}$ is the buoyancy frequency squared (in s^{-2}), $g = 9.81$ m s^{-2} the gravitational acceleration, ρ the density sorted for inversions (in kg m^{-3}), and $\Gamma = 0.2$, the flux parameter, taken here constant [*Osborn*, 1980; *Moum et al.*, 2002, 2004; *Burchard*, 2009; *Rippeth et al.*, 2009; *Holtermann et al.*, 2012]. Turbulent fluxes (F) of any nutrient can be calculated by combining turbulent diffusivity profiles ($K(z)$) and vertical gradient of nutrient concentration with

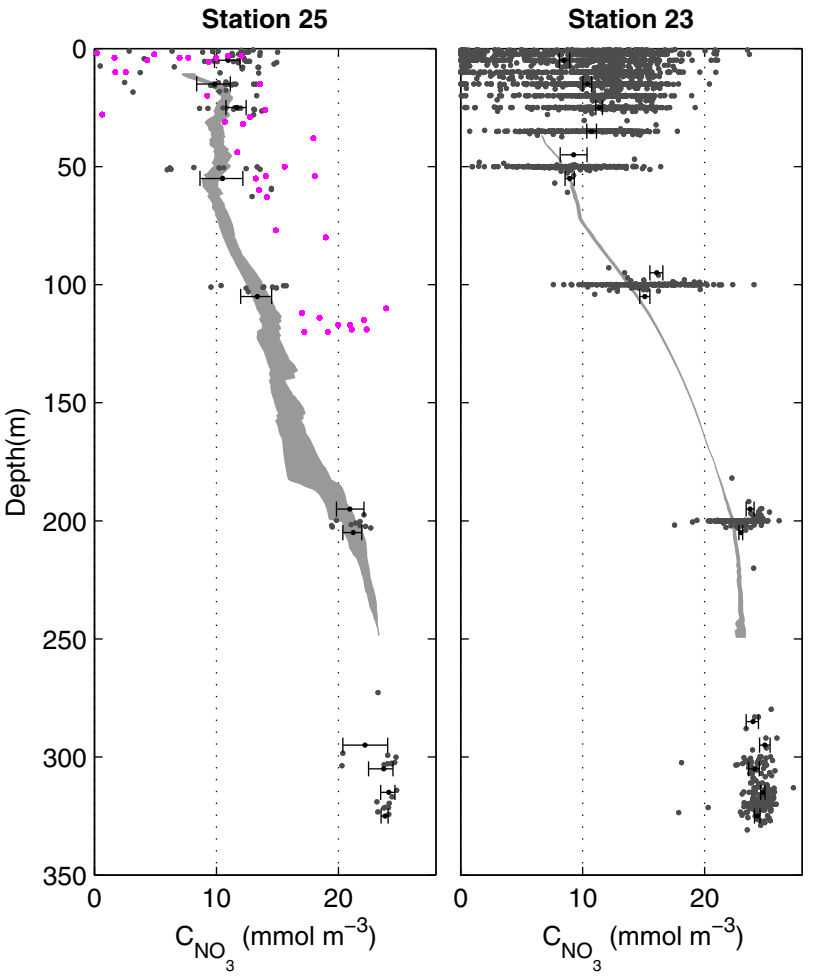

Figure 2. Nitrate concentrations for (left) Stations 25 and (right) 23. Gray dots are all available water bottle samples from 2000 to 2012. Purple dots on Station 25 profiles are the observations from the two campaigns carried out at a fixed station in September 2012. Error bars represent the mean value and its 95% confidence interval obtained from bootstrap analysis in 10 m depth bins. Shaded profiles are fits obtained with equation (3) at Station 23 and at the HLC (the closest VMP sampling to Station 25).

$$F(z) = -K(z)\frac{\partial C(z)}{\partial z}, \tag{3}$$

where $C(z)$ is the nutrient concentration profile. As presented further in the text, nitrate fluxes are calculated here, using the salinity profiles measured by the VMP as proxies for nitrate concentration profiles.

3. Observations

3.1. Nutrient Concentration

Two examples of mean nitrate concentration profiles resulting from our analysis are shown for Stations 25 and 23 (Figure 2). Note that Station 25 has a lower number of observations ($n = 25$, including the September 2012 survey) compared to the monitoring Station 23 ($n = 254$). The result of the bootstrap is shown as error bars where the range is the 95% confidence interval on the mean value. For these two stations in the LSLE, nitrate concentration profiles exhibit a two-layer structure, with nearly constant lower concentrations in the top 50 m of the water column and a constant maximum value below about 200 m. Although the water column is undersampled in the transition zone between these two layers, the gradual decrease of nitrate concentration between 50 and 200 m suggests that the nitracline lies in this depth range.

Binned observations for all stations were vertically and horizontally linearly interpolated between averaged values to obtain a nitrate concentration transect along the Laurentian Channel from Stations 25 to 16

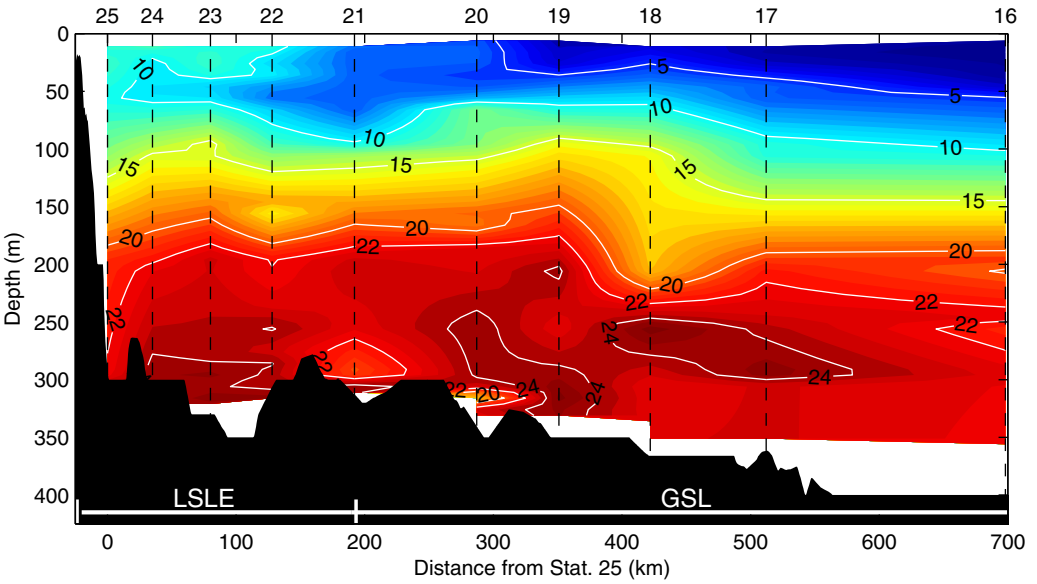

Figure 3. Climatological nitrate concentrations (in mmol m^{-3}) along the Laurentian Channel (April–November, 2000–2012). Dashed-lines represent Stations 25–16 of the transect (see Figure 1).

(Figure 3). Highest surface nutrient concentrations are found in the LSLE (Stations 25–21). Generally low nitrate concentrations are found in surface waters for the rest of the Gulf. Deep (>200 m) waters of the Laurentian Channel have more or less a constant nitrate concentration. There is also a subsurface minimum of nitrate concentration near ∼50 m between Stations 24 and 22. This suggests that high concentration in surface waters is the result of advection of nutrient-rich waters from upstream (i.e., from the HLC) rather than local vertical mixing at these stations.

A look at one of the two 13 h time series near Station 25 gives insights on the behavior of the temperature, salinity, and nitrate concentration at the HLC during a semidiurnal tidal cycle (Figure 4). Visible in temperature and salinity fields is the large vertical excursions reaching up to 60 m. Such large vertical excursions are also visible in the nitrate time series, although the lower temporal resolution of the bottle sampling may be misleading. For example, while the temperature and salinity below 50 m plunge by nearly 60 m between 17:00 and 21:00, nitrate concentration remains constant in the interpolated field because no bottle sample was taken during this period. The relationship between salinity and nitrate concentration was determined by a scatterplot of all available measurements in the GSL/LSLE (Figure 5). The relationship is stronger for data far from the surface and the bottom, i.e., for $S_A \in [32, 34.3]$ g kg^{-1}, for which a linear relationship gives (gray line in Figure 5a):

$$\tilde{C}_{NO_3} = aS_A + b \text{ in } [\text{mmol m}^{-3}], \tag{4}$$

with $a = 7.35$ mmol m^{-3} kg g^{-1} and $b = -227$ mmol m^{-3}. The salinity range used to establish this relationship was selected from visual inspection of the data set and is a trade-off between the goodness of the fit (now with a correlation coefficient $R = 0.94$) and the desire of taking into account the largest portion of the water column. Note that this relation was established for profiles taken between April and November, but the inclusion of winter months does not significantly change the coefficients a and b since the seasonal cycle of nitrate concentration is small for this salinity range (not shown). Near the surface, salinities lower than $S_A = 32$ g kg^{-1} represent the portion of the water column affected by winter mixing and for which the relationship is not expected to hold. At salinities greater than 34.3 g kg^{-1} (i.e., near the bottom), nitrate concentrations have a small tendency to decrease as the salinity increase. This break from the tight nitrate-salinity relation for $S_A \in [32, 34.3]$ g kg^{-1} occurs near a deep temperature maximum that corresponds to a water mass end-member. Waters of higher salinity are a mixture of this end-member with saltier but colder water waters of lower nitrate concentrations. Denitrification may also play a role in the decrease since the

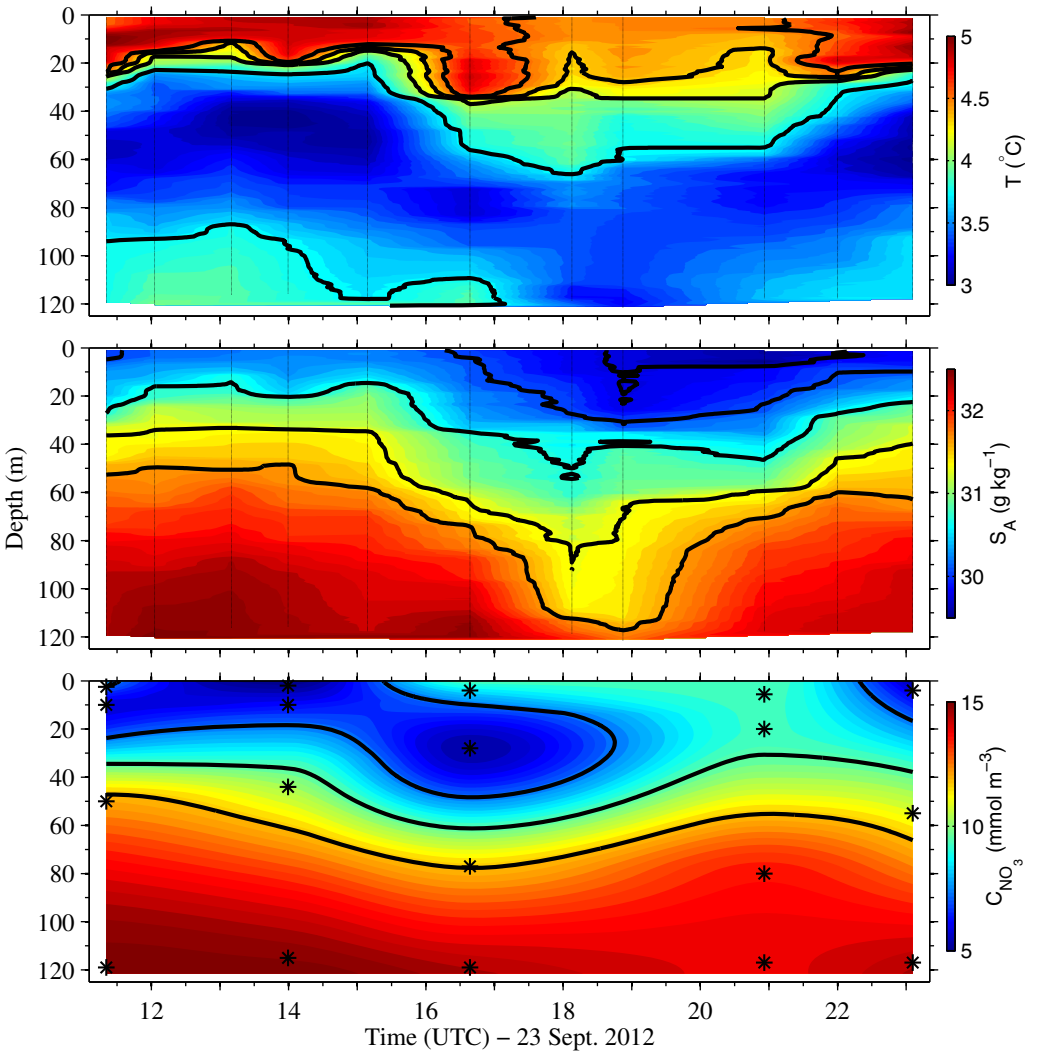

Figure 4. Semidiurnal time series (~13 h) of (top) temperature, (middle) salinity, and (bottom) nitrate concentration for a fixed station occupied on 23 September 2012 (see white star near Station 25 in Figure 1). Temperature-salinity casts are identified with dotted-lines and water sample bottles with black asterisks. The high tide was at 13:03 and the low tide at 19:03. The nearest maximum spring tide occurred on 18 September 2012.

deepest parts of the LSLE are subject to hypoxia. The goodness of the fit for $S_A \in [32, 34.3]$ g kg^{-1} also suggests that this layer is never ventilated throughout its journey from the mouth of the Laurentian Channel to the HLC, i.e., where it is upwelled/mixed.

The relationship established in equation (3) is used to estimate nitrate concentration profiles from VMP casts. Examples of such inferred nitrate concentration estimates are presented in Figure 5b for two profiles from the same semidiurnal tidal cycle, one taken just downstream from the sill (thick lines) and one taken on the shallow portion above the sill (thin lines). Comparison between both salinity profiles (black curves) suggests the profile over the sill is essentially a compressed version of the seaward profile resulting from the advection of the later toward shallower waters. This translates in the nitrate concentration profiles (cyan curves) by changing the depth range for which the relation is valid. For the profile downstream from the sill, the relation fails above 60 m, while above the sill the relation is valid from the bottom (35 m) to a depth of about 15 m. The mean nitrate concentration profiles approximated from the VMP sampling at Station 23 and nearby Station 25 are given in Figure 2 (gray shades).

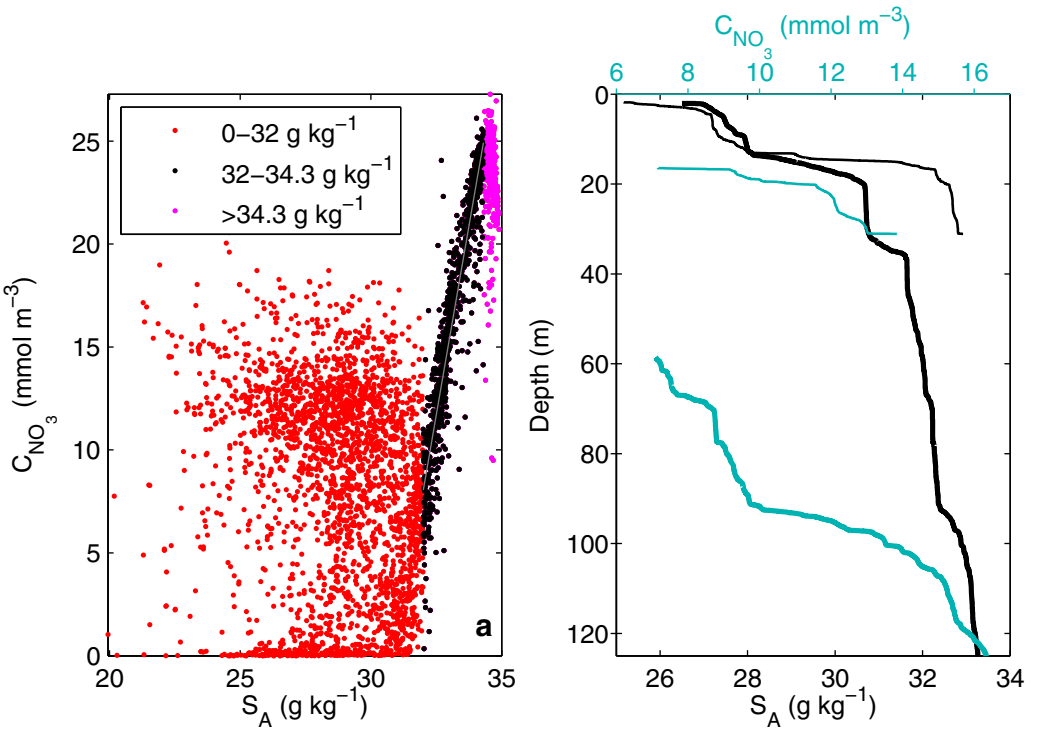

Figure 5. Nitrate concentration relationship with other physical data. (a) Scatterplot of nitrate concentration versus salinity for all 4548 measurements available from all stations. In red, measurements with salinities lower than $S_A = 32$ g kg^{-1}. In magenta, measurements with salinities greater than $S_A = 34.3$ g kg^{-1}. For the 1407 measurements with $S_A = [32, 34.3]$g kg^{-1} (black), the correlation coefficient with a linear least squares fit (thin gray line) gives $R = 0.94$. (b) Salinity profiles (black) from two casts realized on 1 October 2009. In cyan, nitrate profiles inferred from equation (3). The first cast was located in the deep area seaward of the sill at 13:32 (thick lines) and the second above the sill at 18:40 (thin lines). These time references can be found in Figure 6.

Internal tides, well known to be generated at the HLC [e.g., *Forrester*, 1970, 1974; *Ingram*, 1979b; *Wang et al.*, 1991; *Galbraith*, 1992; *Cyr et al.*, 2015], can generate large vertical excursions such as those observed in Figure 4. At this frequency, the internal tide that predominantly emanates from the head is consistent with a Poincaré-type wave in the second vertical mode and first horizontal mode with a wavelength of about 35–60 km [*Forrester*, 1974; *Galbraith*, 1992]. Evidence that the vertical excursions observed for T, S_A, and C_{NO_3} in Figure 4 are the result of an internal tide is suggested by what resembles a pinching and spreading of the isopleths at a node located at a depth of about 20–30 m, typical of a vertical mode-2. The clearest illustration of such behavior is seen the top plot of Figure 4, where isotherms pinching is centered at about 14:00 and spreading is maximum at about 19:00. These occur, respectively, near high and low tides in Tadoussac (respectively, at 13:03 and 19:03). Surface waters are coldest when isotherms located over the node depth rise toward the surface at low tide. Nitrate concentrations are also maximum in surface waters near low tide, likely the result of the same mechanism.

In the salinity field, fresher waters are found in the top ~10 m of the water column at low tide. This is contrary to what might be expected since saltier water should follow the surfacing of colder and nitrate-rich water. An increase in the freshwater release from the St. Lawrence and the Saguenay rivers when the barotropic tidal pressure is minimum (i.e., at low tide) may explain this different behavior as suggested by previous studies [e.g., *Drainville*, 1968; *Saucier and Chassé*, 2000]. In other words, the salt input to the surface water by the vertical mode-2 internal tide is hidden under a more important freshwater release.

3.2. Turbulence Observations and Nitrate Fluxes

A time series of VMP sampling reveals that very high dissipation rates of turbulent kinetic energy occurred above the sill (Figure 6a). In comparison, mixing at a sloping boundary about 100 km seaward from the sill rarely exceeded $\epsilon = 10^{-5}$ W kg^{-1} while above the sill it often exceeded $\epsilon = 10^{-4}$ W kg^{-1} (*Cyr et al.*, 2015). Note that this figure is presented relative to the time of the profiles rather than the alongshore distance. In

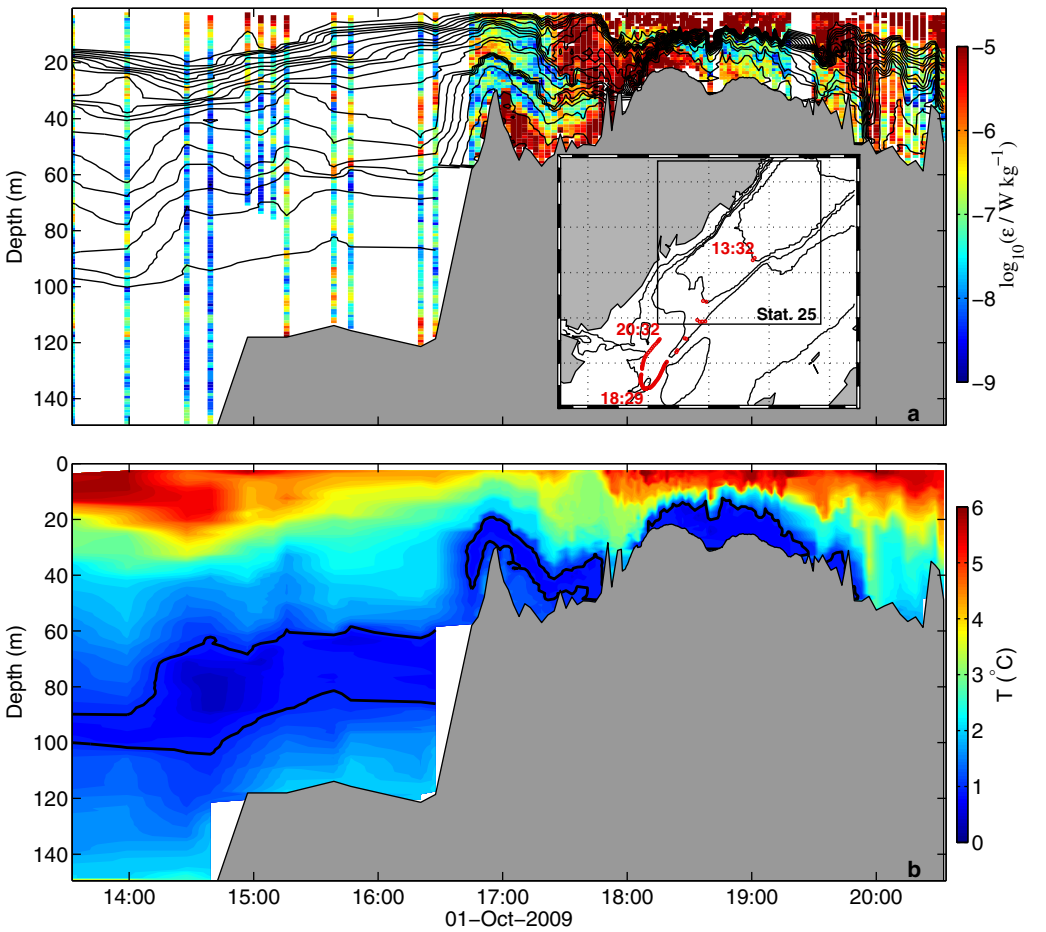

Figure 6. Example of a sampling carried out on 1 October 2009 near Station 25. (a) Dissipation rates of turbulent kinetic energy (ϵ). Isopycnals are also plotted in background for reference. Geographical position of each cast can be roughly followed with the inset figure. (b) Temperature field linearly interpolated between casts. The thick black line is the 1°C isotherm. Except for the shallowest portion of the sill, the gray area for both plots is the maximum depth of the casts which is our best approximation in this rapidly changing topography since casts were performed as close as possible to the seabed (see section 2). On the shallowest portion of the sill, where the maximum depth is less than 35 m, the bottom is that estimated from ADCP measurements.

fact, the tidal currents reversed when the boat was nearly above the shallowest portion of the sill (∼18:45) and the time series from 17:00 to 20:30 is more or less a back and forth displacement above the sill (see the inset for profile positions).

Away from the sill (i.e., before 16:30), dissipation rates were relatively low with some higher patches near the surface and the seabed. As the sill was approached, isopycnals rose by more than 20 m above the first bathymetric peak (at ∼17:00) and plunged behind it. This corresponds to high dissipation rates on the lee side of this peak. These vertical displacements are also visible in the temperature time series (Figure 6b). The CIL (black lines) that lies at a depth of about 90–100 m before 14:00 is pushed over the sill (20–40 m) at about 19:00. Isopycnals are also compressed, generating sharp interfaces where, as will be shown later, turbulence driven by shear instabilities likely take place (Figure 6a). On the shallowest portion of the sill (i.e., after 17:30), most of the water column is highly turbulent. A lens of lighter water appeared at the surface at about 17:45, roughly corresponding to high tide. At this time, we visually observed a well-defined front at the surface. A sharp pycnocline also appears at about 10 m depth, separating two relatively well mixed water masses. Strongest mixing occurred in the upper layer. Visual surface indications of ascending and descending motions were also visible from the boat at ∼20:00 and 20:30. These corresponded to the occurrence of steep isopycnals in parts of the water column (Figure 6a). Vertical *drops* at depths between 10 and 30 m in the temperature panel (Figure 6b) starting at about 17:30 also suggest either high-frequency internal waves or vigorous mixing in the upper part of the water column.

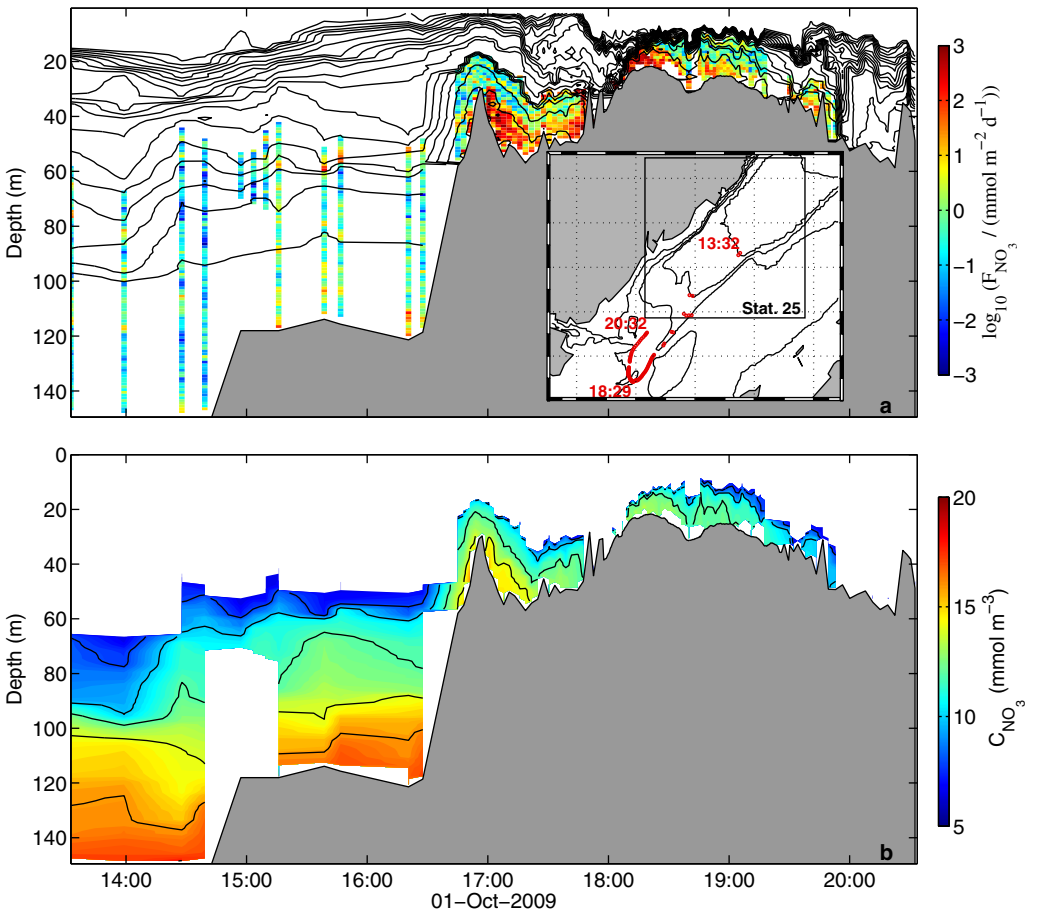

Figure 7. Same sampling as in Figure 6, but for (a) nitrate fluxes (F_{NO_3}) and (b) nitrate concentrations. For both plots, the white portion in the upper part of the figures correspond to the portion of the water column where $S_A < 32\,\mathrm{g\,kg^{-1}}$.

The relationship established in equation (3) was used to infer, for each VMP cast, a corresponding nitrate profile ($\tilde{C}_{NO_3}$). These were then combined with diffusivity profiles to calculate instantaneous fluxes using equation (2) with $F = F_{NO_3}(z)$ and $C(z) = \tilde{C}_{NO_3}$. These are calculated in mmol m^{-2} s^{-1} but expressed further in the text in mmol m^{-2} d^{-1}. Is worth noting that these fluxes still represent instantaneous fluxes, although expressed with units where daily time scales appear.

Figure 7 shows nitrate fluxes and concentrations over the sill. Strong turbulence generally resulted in high nitrate fluxes ($F_{NO_3} \in [10^2, 10^3]$ mmol m^{-2} d^{-1}, Figure 7a). This figure also illustrates how advection/upwelling brings deeper nutrient-rich waters over the sill where they can mix. Nitrate isopleths are also closer to each other over the sill (see also discussion concerning Figure 5b), generating sharper gradients and likely enhancing fluxes. As suggested later in the discussion, the interplay between strong turbulence and the tidal advection of deeper nutrient-rich water above the sill is the key to sustain the high-nutrient fluxes observed here.

Although mixing mechanisms are difficult to isolate from this time series, observations from the 29 September 2012 13 h survey illustrate one turbulent mechanism leading to high-nutrient fluxes at the HLC (Figure 8). This echogram, combined with currents, density, and nitrate observations, shows how Kelvin-Helmholtz instabilities develop at early flood tide (14:35–14:40) as a result of a shear layer centered at about 60 m. The Richardson number $\left(Ri = \frac{N^2}{S^2}\right)$, an index of the water column stability relative to turbulent shear instabilities, suggests that the shear was sufficiently strong to dynamically destabilize the stratification $\left(Ri < \frac{1}{4}\right)$. Here N^2 and S^2 are averaged over 1 m size vertical bins. These conditions led to the development of 30 m thick

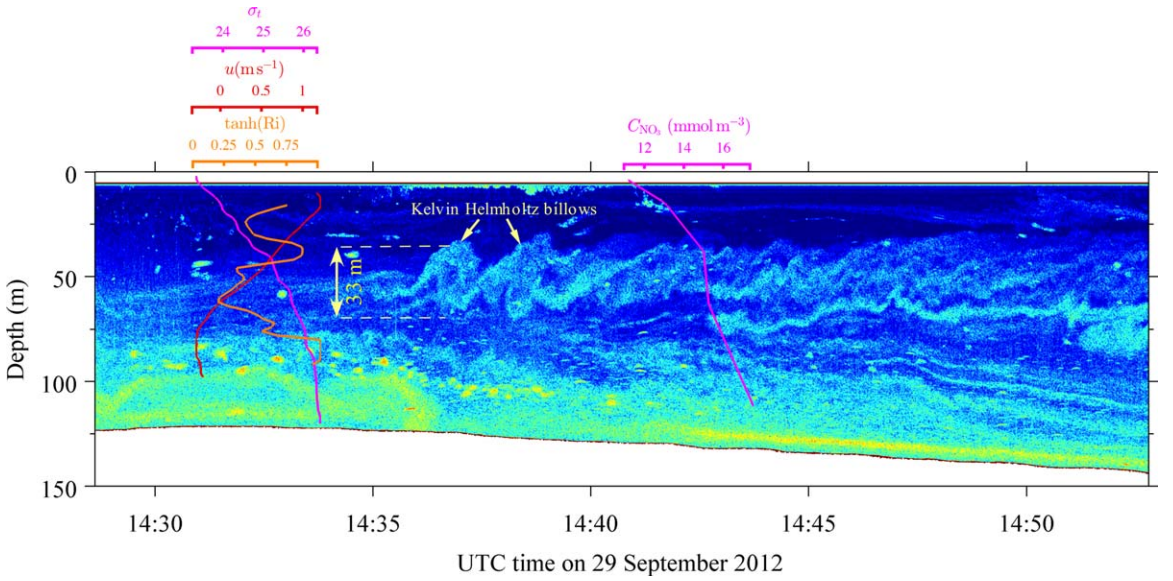

Figure 8. The nutrient pump in action. Echogram at 120 kHz from an echo sounder mounted below a drifting boat on 29 September 2012 (see location in Figure 1) shows how Kelvin-Helmholtz instabilities develop at early flood tide (14:35–14:40). Alongshore currents u (east and north currents rotated by 52°), density (σ_t), gradient Richardson number (Ri), and nitrate concentrations (C_{NO_3}) are also provided. Note that density and nitrate concentration profiles have been linearly interpolated to their respective time from casts outside the limits of the figure. These allow an estimation of the instantaneous vertical nitrate flux (see text).

billows that stirred about a quarter of the water column. Such billows eventually break into turbulent mixing and produce important salt, heat, and nutrient fluxes.

Unfortunately, we do not have concomitant turbulent observations with this echogram. We can nevertheless provide an order of magnitude estimate of the associated diffusivity and nutrient flux from the vertical scale $H \sim 10^1$ m of the billows and the measured buoyancy frequency $N \sim 10^{-2}$ s^{-1}, estimated from the density profile around the shear layer in Figure 8. An order of magnitude calculation suggests a diffusivity of order $K \sim \Gamma N H^2 \sim 10^{-1} \times 10^{-2}\,\mathrm{s^{-1}} \times 10^2\,\mathrm{m^2} \sim 10^{-1}\,\mathrm{m^2\,s^{-1}}$. The associated nutrient flux using $\frac{\partial C_{NO_3}}{\partial z}$ $\sim 10^{-1}$ mmol m^{-4} then suggests $F \sim -K\frac{\partial C_{NO_3}}{\partial z} \sim 10^{-2}\,\mathrm{mmol\,m^{-2}\,s^{-1}}$. This is a high flux (equivalent in other units to $\sim 10^3\,\mathrm{mmol\,m^{-2}\,d^{-1}}$) representative of an episodic but very energetic event.

An example of such episodic events observed during our surveys with the turbulence profiler is provided in Figure 9. This figure is a subset of data from Figure 6 corresponding to the upper 35 m of the water column, between about 17:00 and 20:30. Strong shear layers (top plot) generally correspond to regions of high dissipation (middle plot), delimited from the regions of lower dissipation by strong density gradients. Between 18:00 and 18:15, structures resembling Kelvin-Helmholtz billows are visible in the ADCP echogram. Although these billows are smaller than those presented in Figure 8, VMP casts through them suggest that the nitrate fluxes involved just below these instabilities are of the same order of magnitude, i.e., $F_{NO_3} \sim 10^3$ mmol m^{-2} d^{-1} (bottom plot).

To obtain longer-term averaged quantities, we computed averaged profiles for N^2, ϵ, K, and F_{NO_3} from our 207 casts at the HLC near Station 25 and from our 817 casts at Station 23 (Figure 10). The envelope of these profiles is the bootstrapped 95% confidence interval on the average, calculated assuming log-normal distribution of the turbulent variables [*Baker and Gibson*, 1987]. While sampling at the HLC is slightly biased with more casts near high tide, the sampling at Station 23 is not (see insets in the leftmost plots). This bias is discussed later in the text. Since the VMP sampling is slightly outside the square box of Station 25 (see red dots in Figure 1), these observations are grouped under the tag *HLC* or *Station HLC* to make the clear distinction with Station 25, although they are spatially very close.

The stratification (given by N^2) was nearly the same between Stations HLC and 23, except for the top 25 m, where it was higher at the HLC. The dissipation rates (ϵ) and the diffusivity (K) were higher at the HLC than Station 23 for most of the depth span. The difference is particularly important in the top 60 m of the water

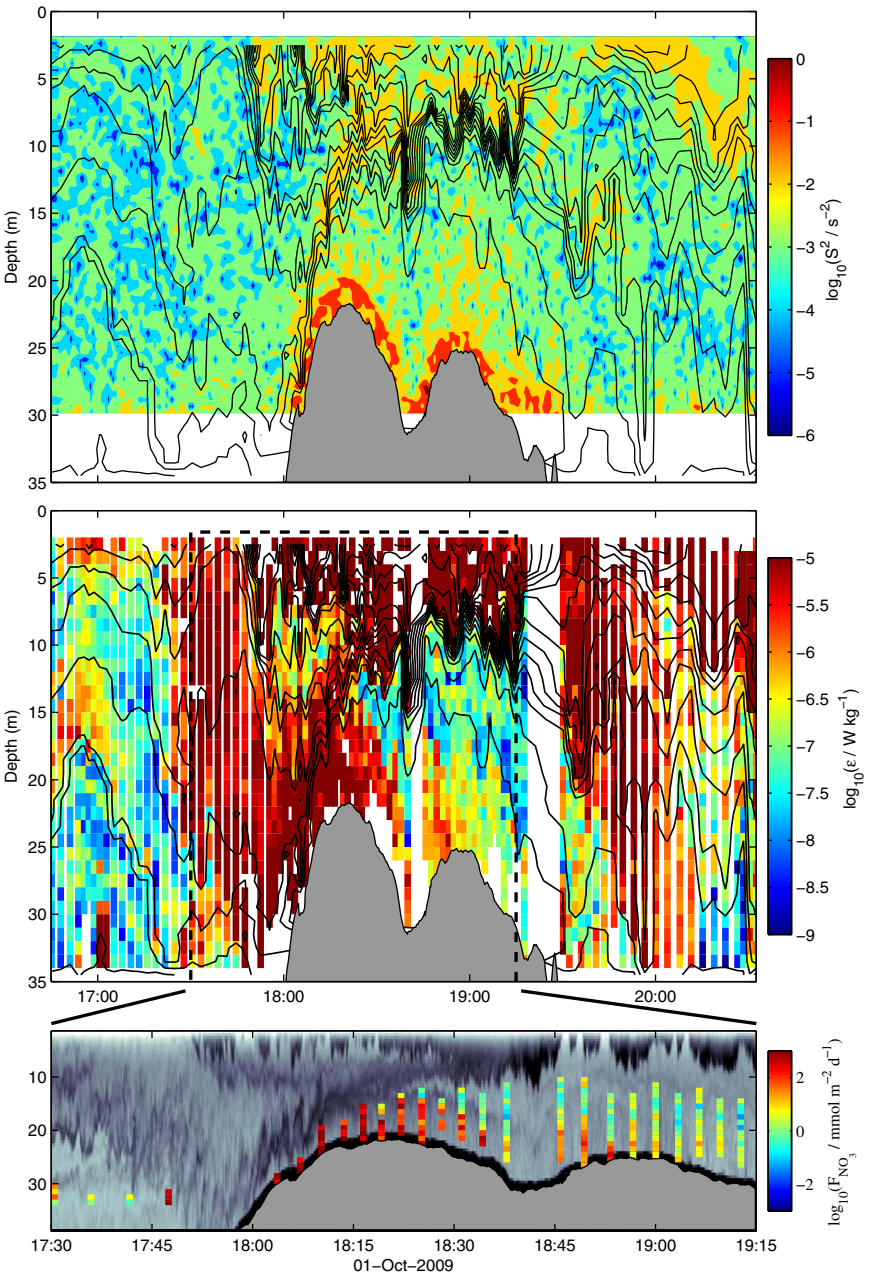

Figure 9. Close-up view of the time series from Figure 6. (top) The shear (S^2) from the ADCP recorder and (middle) the dissipation rates of TKE are presented. (bottom) Enlargement of the middle plot where nitrate fluxes are presented over the ADCP echogram. Note that for a better visualization, the bottom plot is scaled differently from other plots and only one cast out of two is presented. Missing parts of the fluxes profiles correspond to the region where $S_A < 32\,\mathrm{g\,kg^{-1}}$.

column where the diffusivity at the HLC was nearly constant with values near $K \sim 10^{-2}\,\mathrm{m^2\,s^{-1}}$. For the 25–50 m depth range, a range justified further in the text, $\bar{K}_{\mathrm{HLC}} = 4.5(1.1, 13) \times 10^{-2}\,\mathrm{m^2\,s^{-1}}$ and $\bar{K}_{23} = 4.4(2.3, 7.6) \times 10^{-5}\,\mathrm{m^2\,s^{-1}}$, 3 orders of magnitude lower. Here numbers in parentheses represent the bootstrapped 95% confidence interval on the averaged value.

Mean turbulent nitrate fluxes ($F_{\mathrm{NO_3}}$) are also presented in Figure 10. Missing data at the top of the mean profiles represent the portion of the water column where salinities were always lower than 32 g kg^{-1} (i.e., above ~37 m at Station 23 and above ~12 m at the HLC). Fluxes at the HLC were higher than at Station 23 for most of the water column, often by orders of magnitude. Since Figure 2a suggests that the nitrate-

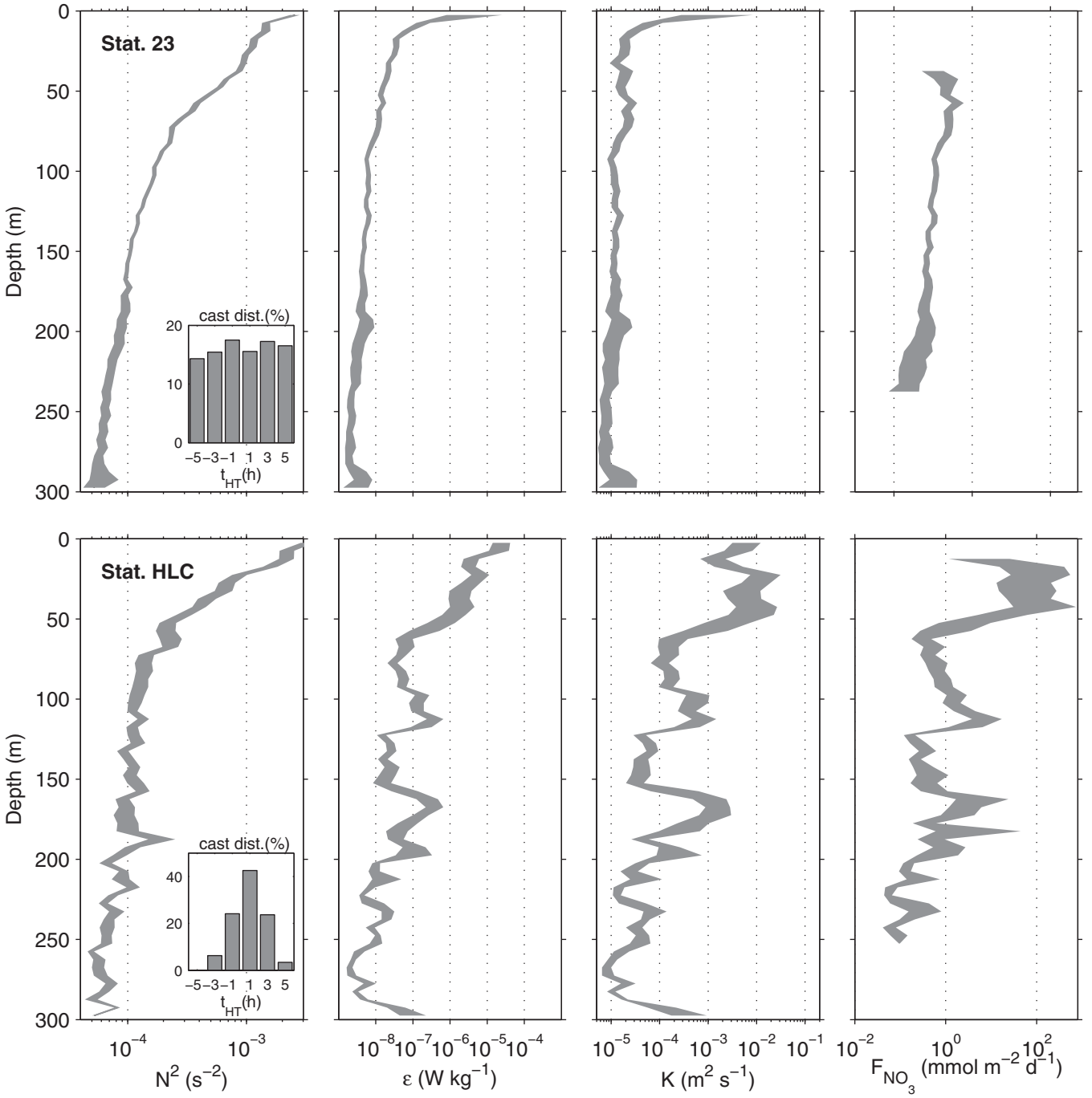

Figure 10. Buoyancy frequency squared (N^2), dissipation rate of TKE (ϵ), turbulent diffusivity (K), and turbulent nitrate flux (F_{NO_3}) for Stations 23 and HLC, respectively. The gray intervals are the 95% confidence interval on the averaged profile. Insets in leftmost plots are the distribution of the casts relative to the closest high tide time ($t_{HT} = 0$ h).

depleted layer roughly corresponds to the top 50 m of the water column, we calculated the mean flux between 25 and 50 m as a measure of replenishment of the surface layer. This depth range is above the nitracline (estimated to lie between 50 and 200 m in section 3.1), but encompasses the limit often considered between the surface and the cold intermediate layer [e.g., *Sinclair et al.*, 1976; *Therriault and Levasseur*, 1985; *Plourde and Runge*, 1993; *Savenkoff et al.*, 2001; *Plourde and Therriault*, 2004]. This interval has also been chosen to represent the flux at the base of the euphotic zone, typically found at a depth of 10–20 in the LSLE [*Therriault and Levasseur*, 1985; *Vézina*, 1994; *Sime-Ngando et al.*, 1995]. The mean fluxes in the 25–

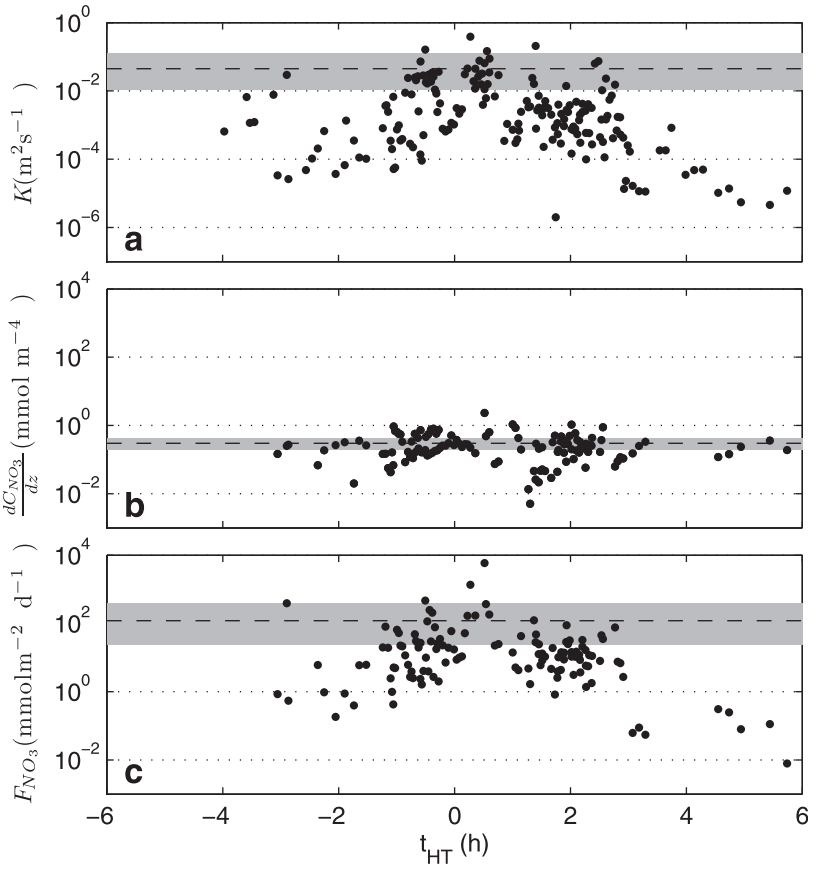

Figure 11. Semidiurnal modulation of the turbulent flux and the terms composing its calculation for observations at the head of the Laurentian Channel. (a) Turbulent diffusivity. (b) Vertical gradient of nitrate concentration. (c) Turbulent nitrate fluxes. Each dot is an average over one VMP cast in the 25–50 m depth range in relation to its phase relative to the time of the closest high tide in Tadoussac ($t_{HT} = 0$ h). The number of points in Figures 11b and 11c are different than in Figure 11a, because for some casts, the relation between S_A and C_{NO_3} was impossible to establish (salinities are out of the range of validity for equation (3)). The average of all observations (horizontal dashed line) and its 95% confidence interval (shaded) are also plotted in each plot. Note that the vertical axes are scaled such that all plots span the same number of orders of magnitude.

50 m depth range, expressed with two significant figures, are $\bar{F}_{HLC} = 120(23, 400)$ mmol m^{-2} d^{-1} and $\bar{F}_{23} = 0.21(0.12, 0.33)$ mmol m^{-2} d^{-1}, respectively, for Stations HLC and 23.

At the transition depth between the bottom layer and the CIL, the nitrate fluxes averaged over the 100–150 m depth ranges were $\bar{F}_{HLC} = 4.2(0.4, 17)$ mmol m^{-2} d^{-1} and $\bar{F}_{23} = 0.15(0.10, 0.24)$ mmol m^{-2} d^{-1}. Note that for fluxes calculations at Station 23, the diffusivity profiles used are from the station itself, i.e., far from the channel sloping boundaries. As suggested by *Cyr et al.* [2011], the fluxes reported for this station could be increased by 60% to account for boundary mixing processes.

4. Discussion

4.1. How Representative Are Fluxes at the HLC?

While fluxes calculated at Station 23 are representative of a long-term research effort (2009–2012) and are not biased toward any tidal phase (semidiurnal or fortnightly), those at the HLC are calculated only from a 4 day campaign. In this section, we explore how representative of the long-term average these fluxes are.

Figure 10 (bottom inset) suggests that the observations at the HLC are biased within a semidiurnal cycle, with more observations in the reversal phase near the high tide ($t_{HT} = 0$ h). A closer look at the flux calculated from single VMP casts suggests that while the vertical nitrate concentration gradients do not change much during a semidiurnal cycle, the turbulent diffusivities and turbulent fluxes are distributed along a bell-shaped curve centered at high tide and spanning orders of magnitude on the vertical axis (Figure 11). The short reversal period between ebb and flood currents thus drives most of the nitrate fluxes at the HLC as

suggested by the averaged values from all our observations (gray shading) that occur toward the top of the curve. Our sampling thus captured the most important phase for the diffusivity and the flux calculations. However, assuming that the statistical distributions presented in Figure 11 are representative of a standard semidiurnal cycle, we can compensate for our observational bias. This can be done by recomputing averages and 95% confidence intervals by taking care that for each bootstrap random replicate, the number of cast in the $t_{HT} \in [-3, 3]$ h interval is approximately the same than in the rest of the semi-diurnal cycle ($t_{HT} < -3$ h or $t_{HT} > 3$ h). For the 25–50 m depth range, this calculation leads to a slightly reduced nitrate flux $\tilde{F}_{HLC} = 95(18, 300)$ mmol m^{-2} d^{-1}. Here the *tilde* symbol denotes correction for sampling bias. For the 100–150 m depth range, the effect is more important with $\tilde{F}_{HLC} = 1.9(0.9, 3.7)$ mmol m^{-2} d^{-1}. For the remainder of the discussion, these corrected flux will be used for Station HLC. Note also that the same correction for the turbulent diffusivity in the 25–50 m depth range at the HLC leads to $\tilde{K}_{HLC} = 8.6(3.2, 19) \times 10^{-3}$ m^2 s^{-1}.

This exercise confirms that most of the flux occurs in a very short period near high tide. The idea that episodic and strong mixing events dominate the averaged fluxes is becoming increasingly recognized, whether for tidal [*Sharples et al*., 2007; *Tweddle et al*., 2013] or for wind mixing events [*Williams et al*., 2013]. It appears that fluxes at the HLC are also driven by episodic mixing events that seem to be occurring principally near high tides. The mechanisms causing such high fluxes will be explored in section 4.2.

It is also worth noting that the survey at the HLC was realized in neap-tide conditions. Historical observations in the LSLE however suggest that nutrient enrichment of the surface waters is more efficient in spring tide conditions [*Ingram*, 1975; *Sinclair*, 1978; *Demers et al*., 1986]. Our estimate of the flux at the HLC may therefore be conservative. The fortnightly difference of mixing in the LSLE was quantified by *Saucier and Chassé* [2000] in a numerical experiment, where they found that the buoyancy fluxes in the LSLE in spring tide are more than the double those in neap tide. If the twofold change in buoyancy fluxes between neap and spring tides reported by *Saucier and Chassé* [2000] translates to the same difference in nitrate fluxes, the nitrate input at the HLC may be higher than our estimate by a factor 1.5.

Finally, how representative are our fluxes measured during the early fall of the extended summer season (i.e., between April and November)? Since the mixing involved here is mostly tidal, we can therefore hypothesize that the energy release is about constant throughout the year, with intrinsic modulations due the different tidal harmonics. It is however possible that variations in the water runoff from the St. Lawrence and the Saguenay rivers may influence the mixing at the HLC. For the spring freshet (April–June), a recent numerical study suggests that increase runoff also increases the vertical buoyancy flux in the LSLE, and thus the vertical resuspension of nutrients [*Saucier et al*., 2009]. However, this hypothesis has never been validated with observations and such a task is beyond the scope of this study. Since for months outside of the spring freshet the runoff is approximately constant on average [*Bourgault and Koutitonsky*, 1999] and because September/October 2009 were close to climatological values (i.e., within one standard deviation of the 30 year climatology) [*Galbraith et al*., 2010], we can therefore assume that our sampling is at least representative of the July–November period.

4.2. The Nutrient Pump Mechanism

Our observations suggest that shear instabilities are one of the mixing mechanisms at work at the HLC. Figure 8 is a good example of such large instabilities driven by sheared currents that can lead to significant nitrate fluxes with overturns as large as 30 m. These instabilities are likely driven by a complex mixture of tidal currents funneled onto the sill, together with frontal activity resulting from the confluence of different water masses (Figures 6 and 8). Internal tides also can generate turbulence by inducing shear in horizontal currents during the vertical displacements of the waves. Bottom friction is another mechanism present at the HLC, as suggested by the high shear and dissipation rates found in the near bottom region of Figure 9.

However, other sill processes are also likely to be encountered here such as lee waves, hydraulic jumps, nonlinear internal waves, vortical structures, etc. [as documented in other similar coastal systems, e.g., *Farmer and Armi*, 1999; *Nash and Moum*, 2001; *Klymak and Gregg*, 2001, 2004; *Armi and Farmer*, 2002; *Cummins et al*., 2003; *Palmer et al*., 2013]. Observational evidence of lee waves has already been reported to occur in this area downstream of the sill as a result of ebb currents [see *Saucier and Chassé*, 2000, Figure 15]. Although mixing through such mechanisms may have been sampled during our campaign (see, for example, isopycnals rising over the sill at 17:00 in Figure 6 that may suggest hydraulic control), our limited

observations likely do not give the complete portrait of turbulence generation at this sill. Although the study would benefit from new turbulence measurements in the area, one conclusion of this short survey is that mixing is high in the upper ~60 m of the water column. Far from the HLC, it is however below this depth that the nitrate concentration starts to increase (see, for example, the mean nitrate profile at Station 23, Figure 2). Without nitrate input closer to the upper layer, mixing would thus not sustain high levels of surface water nitrate enrichment.

In counterpart, some of the mixing mechanisms described above imply large vertical displacements of the nitrate isopleths. The large vertical displacements driven by the barotropic tide forced onto the sill (which further generates internal tides, Figure 4) would not enrich the surface layer with nutrients if no mixing was taking place. Isopleths would instead go up and back down without modifying the mean state. The interplay between vertical displacements and mixing is thus required to sustain the *nutrient pump* since one mechanism alone is not sufficient to account for such high-nutrient fluxes in surface waters. The role of intense vertical mixing near the surface as a necessary condition for nutrient enrichment was hypothesized by *Ingram* [1975] and by *Therriault and Lacroix* [1976] who suggested that vertical displacement of deeper water over the sill by the barotropic tide was not sufficient for the reason mentioned above. Without direct turbulence measurements, *Therriault and Lacroix* [1976] had also hypothesized that the top ~50 m was undergoing intense vertical mixing based on a stratification index at the HLC.

As it was shown previously, a node in vertical displacement is present at a depth of about 20–30 m. Observations suggest that the surface nutrient enrichment by the internal tides occurs in two steps (see sketch in Figure 12). During the pinching of the isopycnals by the internal tide at the node depth, nitrate isopleths from below 60 m rise, enter the zone of vigorous turbulence and enrich the subsurface layer (Figure 12a). When isopycnals diverge, newly enriched waters near the node depth are pushed to the surface by the wave where further mixing ensues (Figure 12b). Near the HLC, this occurs at low tide, consistent with Figure 4 and with previous observations of *Therriault and Lacroix* [1976].

It is suggested in section 4.1 that the calculated nitrate turbulent fluxes at the HLC (18–300 mmol m^{-2} d^{-1}) may be conservative estimates. Yet, they are among the highest reported in the literature (see Table 1). This supports the efficiency of the pumping mechanism described above.

4.3. Contributions to the GSL Nutrient Budget

Sinclair et al. [1976] suggested that nutrient cycling in the LSLE/GSL system was not as hypothesized by *Steven* [1971], whereby the LSLE was acting as a nutrient supplier to the GSL. They rather suggested that the surface estuarine transport of nutrients from the LSLE accounted for less than 1% of the nutrient supply to the GSL and that its effect was geographically limited to the western portion of the Gulf. On the other hand, *Savenkoff et al*. [2001] (from their Figures 6 and 10) calculated by inverse modeling that the nutrient supply to the GSL by the LSLE could reach 40%.

In order to calculate the amount of nitrates brought to the surface during summer months, a surface area representative of the flux at the head of the Laurentian Channel must be calculated. The 25 year sea surface temperature (SST) climatology in the LSLE for the months of May–October, suggests that a cold SST anomaly emanates from the HLC (Figure 13). Since surfacing of deeper nutrient-rich waters should be accompanied by cold water (see, for example, Figure 4), we can therefore assume that the region where nitrate are brought to the surface at the HLC coincides with the coldest part of the SST anomaly. Three contours ($T = 5.35$, 5.55, and 5.65°C, thick black lines in Figure 13) were delimited to represent the area where the fluxes can be hypothesized to occur. They have been chosen to represent 5%, 10%, and 15% of the coldest pixels within the blue box of Figure 13 (calculated from the cumulative density function of temperature pixel in the inset figure). These thresholds give estimated areas of 73, 161, and 230 km^2, respectively. These areas are also visually similar to the *shoaling area* suggested by the numerical work in *Lavoie et al*. [2000, Figure 7). We can therefore assume that $A \sim 10^2$ km^2 is an order of magnitude estimate for the surfacing area representative of the nitrate flux at the HLC. Figure 13 also suggests that surfacing nutrients at the HLC are mostly advected seaward as a part of the estuarine circulation, preferably following the southern coast of the LSLE (see also *Gratton et al*. [1988], for a study on surface cold anomalies).

From May to November (i.e., 150 days), the bias-corrected fluxes $\tilde{F}_{HLC} = 95(18, 300)$ mmol m^{-2} d^{-1} calculated through this surface would lead to an upward pumping of 20 (4, 63) $\times$ 10^3 t of nitrate in the surface

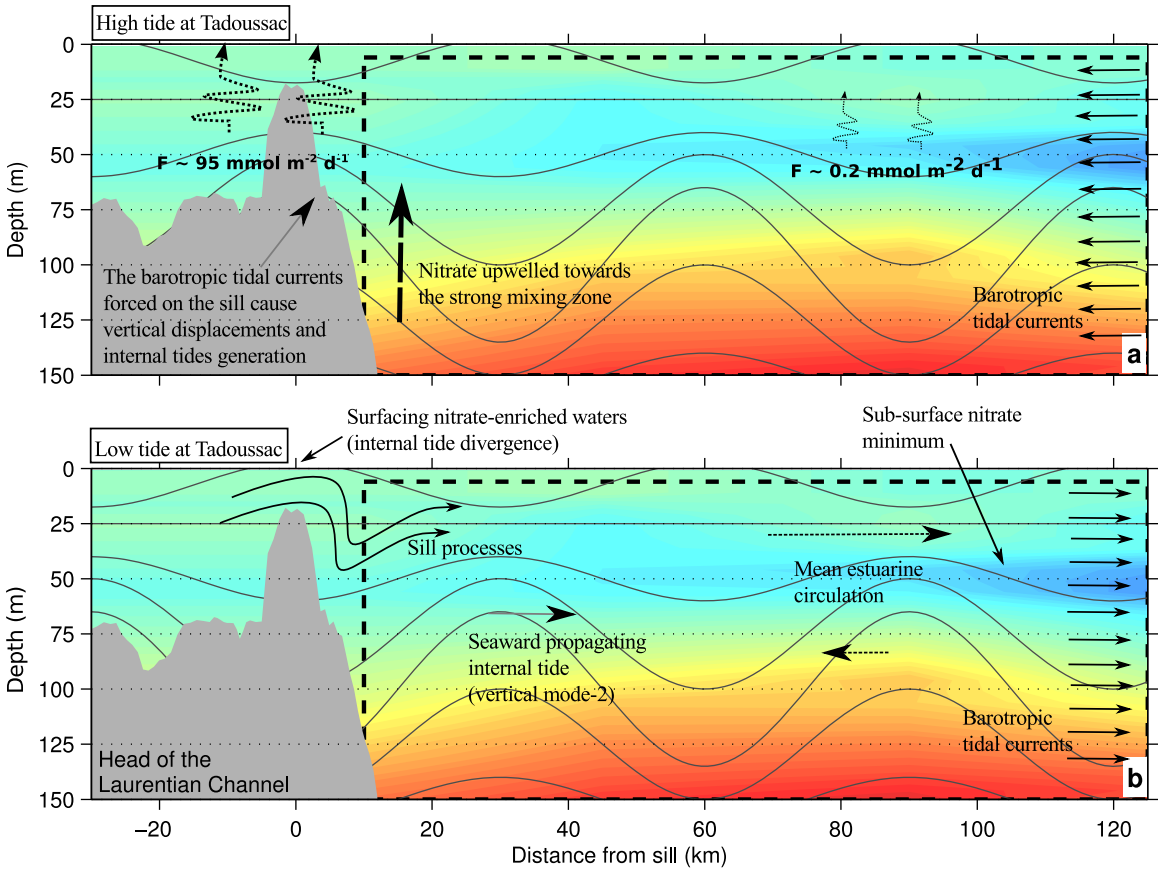

Figure 12. Sketch of some of the processes leading to nitrate fluxes in the LSLE. The color backgrounds represent nitrate concentration on an arbitrary scale, are but based on the average transect of Figure 3 (for data within the dashed rectangle). Outside the dashed rectangle, concentration is extrapolated to the nearest value (no concentration data available from above the sill). Internal tide isopleths heaving for (a) high and (b) low tides at Tadoussac are sketched with thin gray lines for an internal tide of vertical mode-2 with a wavelength of 60 km. Turbulent sill processes are also expected to occur driven by barotropic tidal currents. The interplay between the upwelling of nitrate-rich waters by internal tides and the strong mixing near the sill leads to higher vertical nitrate fluxes (F) at the head of the Laurentian Channel compared to those at the Rimouski Station (located at about 100 km downstream of the sill). (b) Surfacing nitrate-enriched water is advected by the estuarine circulation, creating a subsurface nitrate concentration minimum further downstream. Note that the mean nitrate concentration background is not shown to heave up and down with the internal tide, nor it is shown compressed with isopycnals over the sill.

waters of the LSLE. This amount of nitrate is comparable to the estimated seaward nutrient transport of 20 $\times$ 10^3 t of nitrate over the top 50 m, calculated by *Sinclair et al.* [1976] for the same period at the Rimouski section, a transect across the LSLE passing through Station 23. These authors however pointed out that such a seaward flux was insufficient to sustain the primary production in the Gulf of St. *Law*rence.

Another study from inverse modeling suggests a mean seaward nitrate flux out of the LSLE of 460 mol s^{-1} over the top 30 m, equivalent to 83 $\times$ 10^3 t of nitrate if integrated from May to September, i.e., a little more than our upper bound value [*Savenkoff et al.*, 2001, Figure 6]. Note that this amount of nitrates is *in excess* of what is consumed in the LSLE. The vertical nitrate flux integrated over the entire LSLE given by this inverse model is 685 mol s^{-1} [*Savenkoff et al.*, 2001, Figure 10]. To better compare with this estimate, we should also take into account the vertical fluxes at Station 23, because although they are weaker than at the HLC by two to three orders of magnitude ($\bar{F}_{23} = 0.21(0.12, 0.33)$ mmol m^{-2} d^{-1}), they are representative of a much wider surface area (LSLE surface is $\simeq$ 9000 km^2). If we assume that fluxes at Station 23 are distributed over this surface, and that fluxes at the HLC are distributed over 10^2 km^2, the total vertical nitrate flux over the whole LSLE, expressed in the same units as *Savenkoff et al.* [2001], vary between 33 and 400 mol s^{-1}, i.e., smaller than the model result.

Whether this is an overestimation of the vertical nutrient pumping by the model or whether our results presented here are underestimates is not clear. Additional nitrate sources by the rivers on the north shore of the LSLE may partly account for this difference since they are not considered in the study of

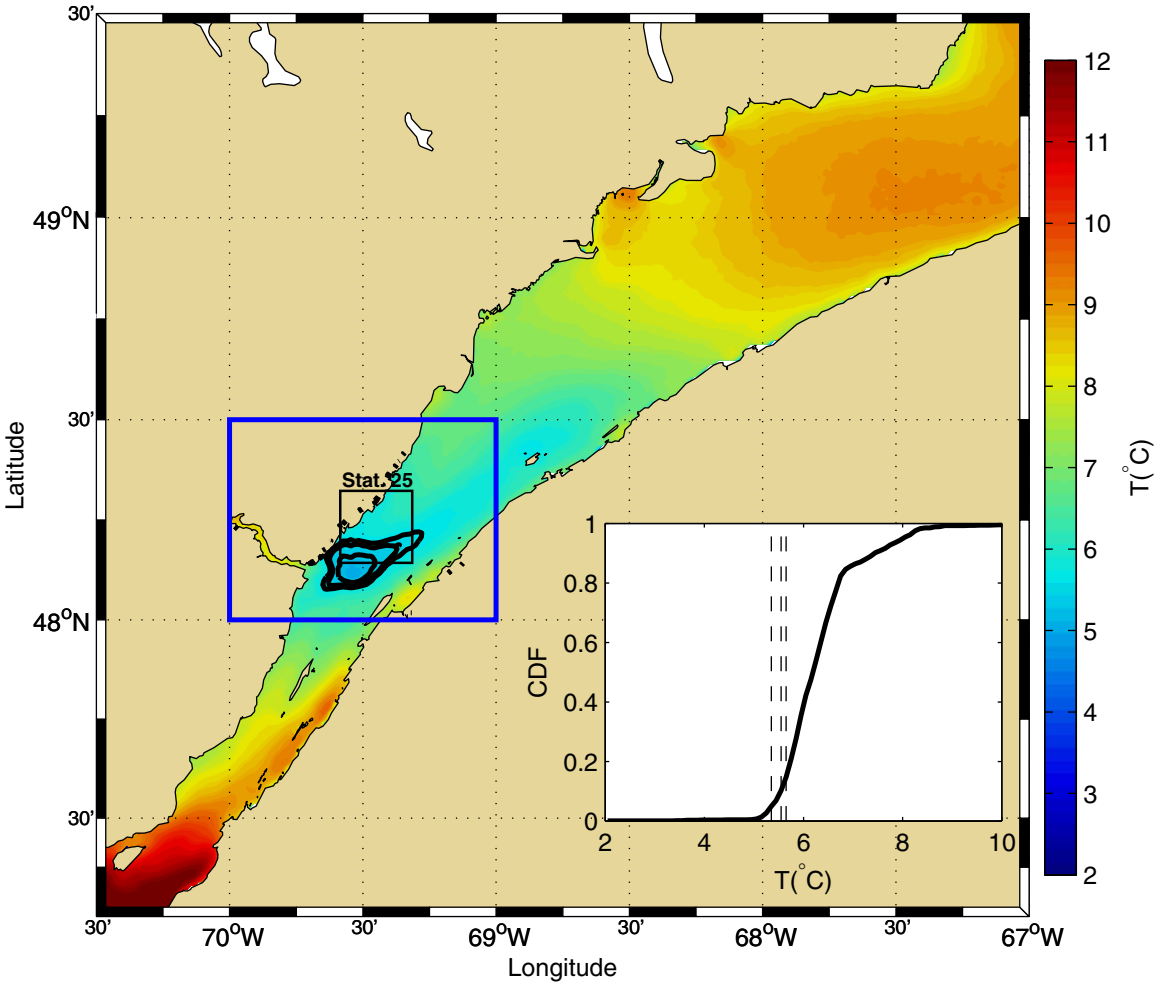

Figure 13. Averaged sea surface temperature from May to October for the 1986–2010 climatology from AVHRR remote sensing at 1.1 km resolution. Black lines correspond to temperature contours $T = 5.35, 5.55, 5.65$°C. These correspond to the coldest pixels (5%, 10%, and 15% in the cumulative density function, inset) within the blue rectangle. Square box around Station 25 from Figure 1 is also shown for reference. These data where obtained from the Maurice Lamontagne Remote Sensing Laboratory and generously provided by P. Larouche.

Savenkoff et al. [2001], and the inverse model may compensate for missing sources by increasing the vertical pumping. Too high local nitrate consumption in the LSLE or too high-nutrient export to the GSL in the model may also cause such overestimation. Note however, in a *best case* scenario, i.e., by considering the largest surface for the shoaling area (e.g., 230 km^2) and by increasing the upper bounds of the 95% confidence interval on $\bar{F}_{\mathrm{HLC}}$ and $\bar{F}_{23}$ by a factor 1.5 and 1.6, respectively (to account for neap-to-spring modulation at HLC and boundary mixing effect in the LSLE), the maximum vertical fluxes would be $\sim$1300 mol s^{-1}, enough to account for *Savenkoff et al*. [2001] results (685 mol s^{-1}). Our results suggest however that the hypothesis from *Sinclair et al*. [1976] is more likely, i.e., that the LSLE plays a relatively minor role in supplying nutrients to the GSL.

4.4. Nutrient Pumping in Sustaining Primary Production in the LSLE

In an attempt to estimate the LSLE primary production that could be sustained by nitrate fluxes at the HLC, let us assume that the nitrate brought to the surface water of the HLC (over $\sim 10^2$ km^2) during a period of 1 month (30 days) is uniformly distributed over the whole LSLE (9000 km^2). The resulting *apparent* nitrate flux for the LSLE is: $F_a = 95(18, 300)$ mmol m^{-2} d^{-1} $\times$ 30d $\times \frac{10^2\ \mathrm{km}^2}{9000\ \mathrm{km}^2} = 32(6, 98)$ mmol m^{-2} mo^{-1}. Given a *Redfield et al*. [1963] uptake ratio by weight (carbon:nitrogen) of 7.7 [see also *Levasseur and Therriault*, 1987; *Levasseur et al*., 1992], this suggests that the nitrate fluxes at the HLC could sustain a carbon (C) production of about $3.4(0.6, 11)$ g C m^{-2} mo^{-1} over the whole LSLE.

Table 1. Turbulent Nitrate Fluxes in the World Ocean From Previous Studies (Updated From *Bourgault et al.* [2011])[a]

Reference	Region	$\bar{F}$ (mmol m^{-2} d^{-1})
Martin et al. [2010]	Porcupine Abyssal Plain	0.09
Lewis et al. [1986]	Subtropical North Atlantic	0.14
Law [2003]	Antarctic Circumpolar Current	0.17
Horne et al. [1996]	Georges Bank	0.047–0.18
Bourgault et al. [2011]	Amundsen Gulf	0.5
Carr et al. [1995]	Equatorial Pacific	0.1–1
Rippeth et al. [2009]	Irish Sea	1.5
Williams et al. [2013]	Celtic Sea (background)	1.3–1.6
Law et al. [2001]	Northern North Atlantic	1.8
Sundfjord et al. [2007]	Barents Sea	0.1–2
Hales et al. [2009]	New England (Shelf Break)	0.8–5
Sharples et al. [2007]	Celtic Sea (Shelf Edge)	1.3–9
Hales et al. [2005]	Oregon Shelf	$\sim 10^1$
Schafstall et al. [2010]	Mauritanian Upwelling Region	10
Li et al. [2012]	California current system (frontal zone)	0–41
Sharples et al. [2001b]	New Zealand Shelf	12
Tweddle et al. [2013]	Celtic Sea (Jones Bank)	0.8–52
Williams et al. [2013]	Celtic Sea (high wind events)	2–81
This study	**Lower St. Lawrence Estuary (sill)**	**18–300**

[a]The values reported are whether the flux through the nitracline, the base of the euphotic zone or the base of the mixed layer and are sorted in terms of the higher-bound estimate.

Estimates of the *total* (i.e., not only nitrate-based) primary production averaged over the whole LSLE are given by *Therriault and Levasseur* [1985] and range between 28 and 44 g C m^{-2} mo^{-1} during the June-July bloom and from 0.3 to 17 g C m^{-2} mo^{-1} for the rest of the year. This suggests that turbulent nitrate fluxes at the HLC can sustain an important part of the bloom and the majority of the postbloom nitrate-based primary production in the LSLE. These results thus reaffirm that nutrient input from the St. Lawrence and the Saguenay rivers plays a modest role in sustaining the primary production [*Greisman and Ingram*, 1977]. These results also suggest that the nutrient fluxes at the HLC are responsible for the high primary production rates found throughout the summer in the LSLE.

Using more recent observations from the monitoring program at Station 23, the mean primary production for years 2000–2003 between May and August (thus including the bloom), varied between 45 and 75 g C m^{-2} mo^{-1} and even reached 150 g C m^{-2} mo^{-1} in 1999 [*Starr et al.*, 2004, Figure 6]. Although these numbers are higher than those presented above, they may however not be representative of the whole LSLE since production is spatially heterogeneous and Station 23 is located in the most productive area [*Therriault and Levasseur*, 1985]. These budgets however reveal that nitrates pumped at the HLC are almost entirely consumed in the LSLE, not leaving much for exportation in the Gulf. This is also suggested by the rapid decrease of nitrate concentration in the surface waters between the LSLE and the GSL (Figure 3). This conclusion also supports the hypothesis that the LSLE exports mostly primary and secondary production to the Gulf rather than nutrients [*Sinclair et al.*, 1976; *Fortier et al.*, 1992; *Plourde and Runge*, 1993].

It must be noted however that the calculation above is based on vertical fluxes derived from measurements in neap-tide period and are likely a lower bound estimate. Again, the total nitrate input to the LSLE, and thus the nitrate-based primary production may be raised by a factor 1.5 to account for the fortnightly difference (see section 3.2). This must be however considered with care and fortnightly changes of nitrate fluxes should be studied more closely. Finally, if fluxes at Station 23 are also taken into account for the total vertical nitrate fluxes, this would lead to an additional flux of $6.3(3.6, 9.9)$ mmol m^{-2} mo^{-1}. This means that turbulent diffusivity far from the HLC, although representative of a much wider area, can only sustain a modest fraction of the total turbulent nutrient fluxes in the LSLE (4–60%, using 95% confidence interval extremes).

5. Conclusion

In a step toward constraining the nutrients cycle and therefore the primary productivity budget in the LSLE/GSL system, nutrient fluxes resulting from strong interaction of the tides with a sill located the upstream limit of the LSLE (the head of the Laurentian Channel) were calculated. Although a better characterization of the mixing processes at the HLC is still required, the mechanics of the pump could be understood as an

interaction between large isopleth heaving over the sill and high dissipation rates in the top 60 m of the water column. Mechanisms leading to the strong dissipation are likely a mixture of shear instabilities, hydraulic controls and water masses convergence driven by internal and barotropic tidal currents funneled on a rough topography.

Calculations of vertical turbulent nitrate fluxes at the head of the Laurentian Channel allow us to put together pieces of the LSLE/GSL nutrient dynamics puzzle that can be summarized as follows. The so-called *nutrient pump* should be better seen as the nutrient supply to the LSLE by the HLC rather than nutrient supply to the GSL by the LSLE as it was first suggested by *Steven* [1971]. Results from this study support the idea that high vertical nutrient fluxes at the HLC can sustain a large fraction of the bloom and postbloom nitrate-based production in the LSLE. This suggests that the nutrients are consumed locally (in the LSLE), leaving few for export to the GSL. The nutrient pump can however have indirect effects on the Gulf by feeding secondary and tertiary producers that can be exported out of the LSLE, mostly via the Gaspé Current.

The role of the LSLE in sustaining vertical fluxes of particulate carbon, and thus carbon sequestration is indeed still an open question. With data from the GSL only, *Rivkin et al*. [1996] concluded that unlike other systems, the gulf exports approximately the same amount of carbon to the bottom whether the surface waters are undergoing bloom or nonbloom conditions. Since the composition of the export is changing from more chlorophyllous material in bloom conditions compared to more fecal pellets in nonbloom conditions, it may well be that the LSLE is a source of biogenic carbon for the GSL throughout the summer. In other words, high primary productivity rates, sustained by high-nutrient input in the LSLE, occur during the whole summer in the LSLE and may feed higher trophic levels that are rapidly exported to the GSL. Such an increase of secondary or tertiary producers may lead to high nonchlorophyllous particulate carbon sinking rates. New information on nutrient fluxes in the LSLE presented here may be used to test this hypothesis in future studies.

Acknowledgments

This work was funded by "Le Fonds de recherche du Québec—Nature et technologies," the Natural Sciences and Engineering Research Council of Canada, the Canada Foundation for Innovation and Fisheries and Oceans Canada and is a contribution to the scientific program of Québec-Océan. The authors would like to thank Pierre Larouche for providing sea surface temperature data sets, Rémi Desmarais and Paul Nicot who were frequent crew members during our summer sampling campaigns, and Cédric Chavanne, Luc Rainville, and two anonymous reviewers for the careful reading and the helpful comments provided. Data used in this study are available either through the St. Lawrence Global Observatory portal (www.slgo.ca) or via the corresponding author (frederic.cyr@nioz.nl).

References

Allen, J., J. R. Siddorn, J. C. Blackford, and F. J. Gilbert (2004), Turbulence as a control on the microbial loop in a temperate seasonally stratified marine systems model, *J. Sea Res.*, *52*(1), 1–20, doi:10.1016/j.seares.2003.09.004.

Armi, L., and D. M. Farmer (2002), Stratified flow over topography: Bifurcation fronts and transition to the uncontrolled state, *Proc. R. Soc. London, Ser. A*, *458*, 513–538.

Arrigo, K. R. (2005), Marine microorganisms and global nutrient cycles, *Nature*, *437*, 349–356, doi:10.1038/nature04159.

Baker, M. A., and C. H. Gibson (1987), Sampling turbulence in the stratified ocean: Statistical consequence of strong intermittency, *J. Phys. Oceanogr.*, *17*(10), 1817–1838.

Banks, R. E. (1966), The cold layer in the Gulf of St. Lawrence, *J. Geophys. Res.*, *71*(6), 1603–1610.

Benoit, J., M. I. El-Sabh, and C. L. Tang (1985), Structure and seasonal characteristics of the Gaspé Current, *J. Geophys. Res.*, *90*(C2), 3225–3236, doi:10.1029/JC090iC02p03225.

Benoit, P., Y. Gratton, and A. Mucci (2006), Modeling of dissolved oxygen levels in the bottom waters of the Lower St. Lawrence Estuary: Coupling of benthic and pelagic processes, *Mar. Chem.*, *102*(1–2), 13–32, doi:10.1016/j.marchem.2005.09.015.

Borges, A. V. (2005), Do we have enough pieces of the jigsaw to integrate CO_2 fluxes in the coastal ocean?, *Estuaries*, *28*(1), 3–27.

Bourgault, D., and V. G. Koutitonsky (1999), Real-time monitoring of the freshwater discharge at the head of the St. Lawrence Estuary, *Atmos. Ocean*, *37*(2), 203–220.

Bourgault, D., C. Hamel, F. Cyr, J.-E. Tremblay, P. S. Galbraith, D. Dumont, and Y. Gratton (2011), Turbulent nitrate fluxes in the Amundsen Gulf during ice-covered conditions, *Geophys. Res. Lett.*, *38*, L15602, doi:10.1029/2011GL047936.

Bourgault, D., F. Cyr, P. S. Galbraith, and E. Pelletier (2012), Relative importance of pelagic and sediment respiration in causing hypoxia in a deep estuary, *J. Geophys. Res.*, *117*, C08033, doi:10.1029/2012JC007902.

Burchard, H. (2009), Combined effects of wind, tide, and horizontal density gradients on stratification in estuaries and coastal seas, *J. Phys. Oceanogr.*, *39*(9), 2117–2136, doi:10.1175/2009JPO4142.1.

Carr, M.-E., M. R. Lewis, D. E. Kelley, and B. Jones (1995), A physical estimate of new production in the equatorial Pacific along 150°W, *Limnol. Oceanogr.*, *40*(1), 138–147.

Chadwick, M., and A. Sinclair (1991), Fisheries production in the Gulf of St. Lawrence, in *The Gulf of St. Lawrence: Small Ocean or Big Estuary?, Can. Spec. Publ. Fish. Aquat. Sci.*, vol. 113, edited by J.-C. Therriault, pp. 125–136, Maurice Lamontagne Institute, Mont-Joli (Qc), Canada.

Clesceri, L. S., A. E. Greenberg, and A. D. Eaton (1989), *Standard Methods for the Examination of Wastewater*, 20th ed., APHA Am. Pub. Health Assoc., Washington, D. C.

Cummins, P. F., S. Vagle, L. Armi, and D. M. Farmer (2003), Stratified flow over topography: Upstream influence and generation of nonlinear internal waves, *Proc. R. Soc. London, Ser. A*, *459*, 1467–1487.

Cyr, F., D. Bourgault, and P. S. Galbraith (2011), Interior versus boundary mixing of a cold intermediate layer, *J. Geophys. Res.*, *116*, C12029, doi:10.1029/2011JC007359.[10.1029/2011JC007359].

Cyr, F., D. Bourgault, and P. S. Galbraith (2015), Behavior and mixing of a cold intermediate layer near a sloping boundary, *Ocean-Dynamics*, *65*(3), p. 357–374, doi:10.1007/s10236-014-0799-1.

de Lafontaine, Y., S. Demers, and J. Runge (1991), Pelagic food web interactions and productivity in the Gulf of St. Lawrence: A perspective, in *The Gulf of St. Lawrence: Small Ocean or Big Estuary?, Can. Spec. Publ. Fish. Aquat. Sci.*, vol. 113, edited by J.-C. Therriault, pp. 99–123, Maurice Lamontagne Institute, Mont-Joli (Qc), Canada.

Demers, S., L. Legendre, and J.-C. Therriault (1986), Phytoplankton responses to vertical tidal mixing, in *Tidal Mixing and Plankton Dynamics*, edited by J. Bowman, M. Yentsch, and W. T. Peterson, pp. 1–40, Springer, Berlin.

Drainville, G. (1968), Le Fjord du Saguenay: 1. Contribution à l'océanographie, *Nat. Can.*, *95*(4), 809–853.

Egbert, G., and R. Ray (2000), Significant dissipation of tidal energy in the deep ocean inferred from satellite altimeter data, *Nature*, *405*(6788), 775–778.

El-Sabh, M. I. (1979), The Lower St. Lawrence Estuary as a physical oceanographic system, *Nat. Can.*, *106*, 55–73.

Falkowski, P. (2000), The global carbon cycle: A test of our knowledge of earth as a system, *Science*, *290*, 291–296, doi:10.1126/science.290.5490.291.

Farmer, D., and L. Armi (1999), The generation and trapping of solitary waves over topography, *Science*, *283*, 188–190.

Fisheries and Oceans—Canada (2013), *Oceanographic Data Management System*, Maurice Lamontagne Inst., Mont-Joli, Quebec, Canada. [Available at http://www.osl.gc.ca/sgdo, last accessed on 16 Aug. 2013.]

Forrester, W. D. (1970), Geostrophic approximation in the St. Lawrence Estuary, *Tellus*, *XXII*(1), 53–65.

Forrester, W. D. (1974), Internal tides in the St. Lawrence Estuary, *J. Mar. Res.*, *32*(1), 55–66.

Fortier, L., M. E. Levasseur, R. Drolet, and J.-C. Therriault (1992), Export production and the distribution of fish larvae and their prey in a coastal jet frontal region, *Mar. Ecol. Prog. Ser.*, *85*, 203–218, doi:10.3354/meps085203.

Galbraith, P. S. (1992), Relating overturns to mixing and buoyancy flux, PhD thesis, Dalhousie Univ., Halifax (NS), Canada.

Galbraith, P. S. (2006), Winter water masses in the Gulf of St. Lawrence, *J. Geophys. Res.*, *111*, C06022, doi:10.1029/2005JC003159.

Galbraith, P. S., R. Pettipas, J. Chassé, D. Gilbert, P. Larouche, B. Pettigrew, A. Gosselin, L. Devine, and C. Lafleur (2010), Physical oceanographic conditions in the Gulf of St. Lawrence in 2009, *Res. Doc.* 2010/035, iv + 73 pp., DFO Can. Sci. Advis. Secr., Ottawa (ON), Canada.

Galbraith, P. S., J. Chassé, D. Gilbert, P. Larouche, C. Caverhill, D. Lefaivre, D. Brickman, B. Pettigrew, L. Devine, and C. Lafleur (2014), Physical oceanographic conditions in the Gulf of St. Lawrence in 2013, *Res. Doc.* 2014/062, vi + 84 pp., DFO Can. Sci. Advis. Secr., Ottawa (ON), Canada.

Gattuso, J.-P., M. Frankignoulle, and R. Wollast (1998), Carbon and carbonate metabolism in coastal aquatic ecosystem, *Annu. Rev. Ecol. Evol. Syst.*, *29*, 405–434.

Gilbert, D., and B. Pettigrew (1997), Interannual variability (1948–1994) of the CIL core temperature in the Gulf of St. Lawrence, *Can. J. Fish. Aquat. Sci.*, *54*(S1), 57–67, doi:10.1139/cjfas-54-S1-57.

Gilbert, D., B. Sundby, C. Gobeil, A. Mucci, and G.-H. Tremblay (2005), A seventy-two-year record of diminishing deep-water oxygen in the St. Lawrence estuary: The northwest Atlantic connection, *Limnol. Oceanogr.*, *50*(5), 1654–1666, doi:10.4319/lo.2005.50.5.1654.

Grasshoff, K., M. Ehrhardt, and K. Kremling (1999), *Methods of Seawater Analysis*, 3rd ed., Wiley, N. Y.

Gratton, Y., G. Mertz, and J. A. Gagné (1988), Satellite observations of tidal upwelling and mixing in the St. Lawrence Estuary, *J. Geophys. Res.*, *93*(C6), 6947–6954.

Greisman, P., and R. G. Ingram (1977), Nutrient distribution in the St. Lawrence Estuary, *J. Fish. Res. Board Can.*, *34*, 2117–2123.

Hales, B., J. N. Moum, P. Covert, and A. Perlin (2005), Irreversible nitrate fluxes due to turbulent mixing in a coastal upwelling system, *J. Geophys. Res.*, *110*, C10S11, doi:10.1029/2004JC002685.

Hales, B., R. D. Vaillancourt, L. Prieto, J. Marra, R. Houghton, and D. Hebert (2009), High-resolution surveys of the biogeochemistry of the New England shelfbreak front during Summer, 2002, *J. Mar. Syst.*, *78*(3), 426–441, doi:10.1016/j.jmarsys.2008.11.024.

Holtermann, P. L., L. Umlauf, T. Tanhua, O. Schmale, G. Rehder, and J. J. Waniek (2012), The Baltic Sea tracer release experiment: 1. Mixing rates, *J. Geophys. Res.*, *117*, C01021, doi:10.1029/2011JC007445.

Horne, E. P., J. W. Loder, C. E. Naime, and N. S. Oakey (1996), Turbulence dissipation rates and nitrate supply in the upper water column on Georges Bank, *Deep Sea Res., Part II*, *43*(7–8), 1683–1712, doi:10.1016/S0967-0645(96)00037-9.

Ingram, R. G. (1975), Influence of tidal-induced vertical mixing on primary productivity in the St. Lawrence Estuary, in *Mémoires de la Société Royale des Sciences de Liège*, edited by J. C. J. Nihoul, pp. 59–74, Univ. of Liege, Liege, Belgium.

Ingram, R. G. (1979a), Water mass modification in the St. Lawrence Estuary, *Nat. Can.*, *106*, 45–54.

Ingram, R. G. (1979b), Internal wave observation off Isle Verte, *J. Mar. Res.*, *36*, 715–724.

Ingram, R. G. (1983), Vertical mixing at the head of the Laurentian Channel, *Estuarine Coastal Shelf Sci.*, *16*(3), 333–338.

Klymak, J. M., and M. C. Gregg (2001), Three-dimensional nature of flow near a sill, *J. Geophys. Res.*, *106*(C10), 22,295–22,311.

Klymak, J. M., and M. C. Gregg (2004), Tidally generated turbulence over the Knight Inlet sill, *J. Phys. Oceanogr.*, *34*(5), 1135–1151.

Koutitonsky, V. G., and G. L. Bugden (1991), The physical oceanography of the Gulf of St. Lawrence: A review with emphasis on the synoptic variability of the motion, in *The Gulf of St. Lawrence: Small Ocean or Big Estuary?, Can. Spec. Publ. Fish. Aquat. Sci.*, vol. 113, edited by J.-C. Therriault, pp. 57–90, Maurice Lamontagne Institute, Mont-Joli (Qc), Canada.

Lavoie, D., Y. Simard, and F. J. Saucier (2000), Aggregation and dispersion of krill at channel heads and shelf edges: The dynamics in the Saguenay—St. Lawrence Marine Park, *Can. J. Fish. Aquat. Sci.*, *57*, 1853–1869.

Law, C. S. (2003), Vertical eddy diffusion and nutrient supply to the surface mixed layer of the Antarctic Circumpolar Current, *J. Geophys. Res.*, *108*(C8), 3272, doi:10.1029/2002JC001604.

Law, C. S., A. P. Martin, M. I. Liddicoat, A. J. Watson, K. J. Richards, and E. M. S. Woodward (2001), A Lagrangian F_6 tracer study of an anticyclonic eddy in the North Atlantic: Patch evolution, vertical mixing and nutrient supply to the mixed layer, *Deep Sea Res., Part II*, *48*, 705–724.

Lehmann, M. F., B. Barnett, Y. Ge, D. Gilbert, R. J. Maranger, A. Mucci, B. Sundby, and B. Thibodeau (2009), Aerobic respiration and hypoxia in the Lower St. Lawrence Estuary: Stable isotope ratios of dissolved oxygen constrain oxygen sink partitioning, *Limnol. Oceanogr.*, *54*(6), 2157–2169.

Levasseur, M. E., and J.-C. Therriault (1987), Phytoplankton biomass and nutrient dynamics in a tidally induced upwelling: The role of the NO_3:SiO_4 ratio, *Mar. Ecol. Prog. Ser.*, *39*, 87–97.

Levasseur, M. E., J.-C. Therriault, and L. Legendre (1984), Hierarchical control of phytoplankton succession by physical factors, *Mar. Ecol. Prog. Ser.*, *19*, 211–222.

Levasseur, M. E., L. Fortier, J.-C. Therriault, and P. Harrison (1992), Phytoplankton dynamics in a coastal jet frontal region, *Mar. Ecol. Prog. Ser.*, *86*, 283–295, doi:10.3354/meps086283.

Lewis, M. R., W. G. Harrison, N. S. Oakey, D. Hebert, and T. Platt (1986), Vertical nitrate fluxes in the oligotrophic ocean, *Science*, *234*(4778), 870–873, doi:10.1126/science.234.4778.870.

Li, Q. P., P. J. S. Franks, M. D. Ohman, and M. R. Landry (2012), Enhanced nitrate fluxes and biological processes at a frontal zone in the southern California current system, *J. Plankton Res.*, *34*(9), 790–801, doi:10.1093/plankt/fbs006.

Lueck, R. G., F. Wolk, and H. Yamasaki (2002), Oceanic velocity microstructure measurements in the 20th century, *J. Oceanogr.*, *58*, 153–174.

Martin, A. P., M. I. Lucas, S. C. Painter, R. Pidcock, H. Prandke, H. Prandke, and M. C. Stinchcombe (2010), The supply of nutrients due to vertical turbulent mixing: A study at the Porcupine Abyssal Plain study site in the northeast Atlantic, *Deep Sea Res., Part II*, *57*(15), 1293–1302, doi:10.1016/j.dsr2.2010.01.006.

McDougall, T. J., and P. M. Barker (2011), *Getting started with TEOS-10 and the Gibbs Seawater (GSW) Oceanographic Toolbox, SCOR/IAPSO WG127*, 28 pp. [Available at www.teos-10.org.]

Mitchell, M. R., G. Harrison, K. Pauley, A. Gagné, G. Maillet, and P. Strain (2002), Atlantic zonal monitoring program sampling protocol, *Can. Tech. Rep. Hydrogr. Ocean Sci. 223*, iv + 23 pp, Bedford Institute of Oceanography, Dartmouth (NS), Canada.

Moum, J. N., D. R. Caldwell, J. D. Nash, and G. D. Gunderson (2002), Observations of boundary mixing over the continental slope, *J. Phys. Oceanogr.*, *32*(7), 2113–2130, doi:10.1175/1520-0485(2002)032<2113:OOBMOT>2.0.CO;2.

Moum, J. N., A. Perlin, J. M. Klymak, M. D. Levine, T. Boyd, and P. Kosro (2004), Convectively driven mixing in the bottom boundary layer, *J. Phys. Oceanogr.*, *34*(10), 2189–2202.

Muller-Karger, F. E. (2005), The importance of continental margins in the global carbon cycle, *Geophys. Res. Lett.*, *32*, L01602, doi:10.1029/2004GL021346.

Nash, J. D., and J. N. Moum (2001), Internal hydraulic flows on the continental shelf: High drag states over a small bank, *J. Geophys. Res.*, *106*(C3), 4593–4611.

Osborn, T. (1980), Estimates of the local rate of vertical diffusion from dissipation measurements, *J. Phys. Oceanogr.*, *10*(1), 83–89.

Ouellet, P., A. Olga, V. Bui, D. Lavoie, J. Chassé, N. Lambert, N. Ménard, and P. Sirois (2013), Seasonal distribution, abundance, and growth of larval capelin (*Mallotus villosus*) and the role of the Lower St. Lawrence Estuary (Gulf of St. Lawrence, Canada) as a nursery area, *Can. J. Fish. Aquat. Sci.*, *70*, 1–23.

Palmer, M. R., M. E. Inall, and J. Sharples (2013), The physical oceanography of Jones Bank: A mixing hotspot in the Celtic Sea, *Prog. Oceanogr.*, *117*, 9–24, doi:10.1016/j.pocean.2013.06.009.

Plourde, J., and J.-C. Therriault (2004), Climate variability and vertical advection of nitrates in the Gulf of St. Lawrence, Canada, *Mar. Ecol. Prog. Ser.*, *279*, 33–43, doi:10.3354/meps279033.

Plourde, S., and J. A. Runge (1993), Reproduction of the planktonic copepod *Calanus finmarchicus* in the Lower St. Lawrence Estuary: Relation to the cycle of phytoplankton production and evidence for a *Calanus* pump, *Mar. Ecol. Prog. Ser.*, *102*, 217–227, doi:10.3354/meps102217.

Plourde, S., P. Joly, J. A. Runge, B. Zakardjian, and J. J. Dodson (2001), Life cycle of *Calanus finmarchicus* in the lower St. Lawrence Estuary: The imprint of circulation and late timing of the spring phytoplankton bloom, *Can. Data Rep. Fish. Ocean Sci.*, *58*(4), 647–658.

Plourde, S., P. Joly, L. St-Amand, and M. Starr (2008), La station de monitorage de Rimouski: Plus de 400 visites et 18 ans de monitorage et de recherche, *Atl. Zone Monit. Program Bull.*, *8*, 51–55.

Redfield, A. C., B. H. Ketchum, and F. A. Richards (1963), The influence of organisms on the composition of sea water, in *The Sea*, vol. *2*, pp. 26–77, John Wiley & Sons, N. Y.

Richardson, K., A. Visse, and F. Pedersen (2000), Subsurface phytoplankton blooms fuel pelagic production in the, *J. Plankton Res.*, *22*(9), 1663–1671.

Rippeth, T. P. (2005), Mixing in seasonally stratified shelf seas: A shifting paradigm, *Philos. Trans. R. Soc. A*, *363*(1837), 2837–2854, doi:10.1098/rsta.2005.1662.

Rippeth, T. P., P. Wiles, M. R. Palmer, J. Sharples, and J. Tweddle (2009), The diapcynal nutrient flux and shear-induced diapcynal mixing in the seasonally stratified western Irish Sea, *Cont. Shelf Res.*, *29*(13), 1580–1587, doi:10.1016/j.csr.2009.04.009.

Rivkin, R., et al. (1996), Vertical flux of biogenic carbon in the ocean: Is there food web control?, *Science*, *272*(5265), 1163–1166.

Saucier, F. J., and J. Chassé (2000), Tidal circulation and buoyancy effects in the St. Lawrence Estuary, *Atmos. Ocean*, *38*(4), 505–556.

Saucier, F. J., F. Roy, S. Senneville, G. C. Smith, D. Lefaivre, B. Zakardjian, and J.-F. Dumais (2009), Modélisation de la circulation dans l'estuaire et le golfe du Saint-Laurent en réponse aux variations du débit d'eau douce et des vents, *Rev. Sci.*, *22*(2), 159–176, doi:10.7202/037480ar.

Savenkoff, C., A. F. Vézina, P. Smith, and G. Han (2001), Summer transports of nutrients in the Gulf of St. Lawrence estimated by inverse modelling, *Estuarine Coastal Shelf Sci.*, *52*(5), 565–587, doi:10.1006/ecss.2001.0774.

Schafstall, J., M. Dengler, P. Brandt, and H. Bange (2010), Tidal-induced mixing and diapycnal nutrient fluxes in the Mauritanian upwelling region, *J. Geophys. Res.*, *115*, C10014, doi:10.1029/2009JC005940.

Sharples, J., C. M. Moore, T. P. Rippeth, P. M. Holligan, D. J. Hydes, N. R. Fisher, and J. H. Simpson (2001a), Phytoplankton distribution and survival in the thermocline, *Limnol. Oceanogr.*, *46*(3), 486–496, doi:10.4319/lo.2001.46.3.0486.

Sharples, J., C. M. Moore, and R. Abraham (2001b), Internal tide dissipation, mixing, and vertical nitrate flux at the shelf edge of NE New Zealand, *J. Geophys. Res.*, *106*(C7), 14,069–14,081.

Sharples, J., J. F. Tweddle, J. A. M. Green, and M. R. Palmer (2007), Spring-neap modulation of internal tide mixing and vertical nitrate fluxes at a shelf edge in summer, *Limnol. Oceanogr.*, *52*(2), 1735–1747.

Sime-Ngando, T., M. Gosselin, S. Roy, and J.-P. Chanut (1995), Significance of planktonic ciliated protozoa in the Lower St. Lawrence Estuary: Comparison with bacterial, phytoplankton, and particulate organic carbon, *Aquat. Microb. Ecol.*, *9*, 243–258.

Sinclair, M. (1978), Summer phytoplankton variability in the Lower St. Lawrence Estuary, *J. Fish. Res. Board Can.*, *35*, 1171–1185.

Sinclair, M., M. I. El-Sabh, and J.-R. Brindle (1976), Seaward nutrient transport in the Lower St. Lawrence Estuary, *J. Fish. Res. Board Can.*, *33*, 1271–1277.

Smith, G. C., F. J. Saucier, and D. Straub (2006), Formation and circulation of the cold intermediate layer in the Gulf of Saint Lawrence, *J. Geophys. Res.*, *111*, C06011, doi:10.1029/2005JC003017.

Starr, M., L. St-Amand, L. Devine, L. Bérard-Therriault, and P. S. Galbraith (2004), State of phytoplankton in the Estuary and Gulf of St. Lawrence during 2003, *Res. Doc.* 2004/123, ii + 31 pp., Can. Sci. Advis. Secr. Fish. Oceans Can., Ottawa (ON), Canada.

Steven, D. M. (1971), International Biological Program study of the Gulf of St. Lawrence, in *Proceedings of the 2nd Gulf of St. Lawrence Workshop*, edited by E. M. Hassan, pp. 146–159, Bedford Inst. of Oceanogr., Dartmouth, N. H., Canada.

Steven, D. M. (1974), Primary and secondary production in the Gulf of St. Lawrence, *Rep. 26*, McGill Univ., Mar. Sci. Cent., Montreal (Qc), Canada.

Sundfjord, A., I. Fer, Y. Kasajima, and H. Svendsen (2007), Observations of turbulent mixing and hydrography in the marginal ice zone of the Barents Sea, *J. Geophys. Res.*, *112*, C05008, doi:10.1029/2006JC003524.

Tang, C. L. (1980), Mixing and circulation in the northwestern Gulf of St. Lawrence: A study of a buoyancy driven current system, *J. Geophys. Res.*, *25*, 2787–2796.

Therriault, J.-C., and G. Lacroix (1976), Nutrients, chlorophyll, and internal tides in the St. Lawrence Estuary, *J. Fish. Res. Board Can.*, *33*, 2747–2757.

Therriault, J.-C., and M. E. Levasseur (1985), Control of phytoplankton production in the Lower St. Lawrence Estuary: Light and freshwater runoff, *Nat. Can.*, *112*, 77–96.

Thomas, H., Y. Bozec, K. Elkalay, and H. J. W. de Baar (2004), Enhanced open ocean storage of CO_2 from shelf sea pumping, *Science*, *304*, 1005–1008, doi:10.1126/science.1095491.

Tsunogai, S., S. Watanabe, and T. Sato (1999), Is there a "continental shelf pump" for the absorption of atmospheric CO_2, *Tellus, Ser. B*, *51*, 701–712.

Tweddle, J. F., J. Sharples, M. R. Palmer, K. Davidson, and S. McNeill (2013), Enhanced nutrient fluxes at the shelf sea seasonal thermocline caused by stratified flow over a bank, *Prog. Oceanogr.*, *117*, 37–47, doi:10.1016/j.pocean.2013.06.018.

Vézina, A. F. (1994), Mesoscale variability in nitrogen uptake rates and the f-ratio during a coastal phytoplankton bloom, *Limnol. Oceanogr.*, *39*(4), 854–868.

Wang, J., R. G. Ingram, and L. A. Mysak (1991), Variability of internal tides in the Laurentian Channel, *J. Geophys. Res.*, *96*(C9), 16,859–16,875, doi:10.1029/91JC01580.

Williams, C., J. Sharples, C. Mahaffey, and T. Rippeth (2013), Wind-driven nutrient pulses to the subsurface chlorophyll maximum in seasonally stratified shelf seas, *Geophys. Res. Lett.*, *40*, 5467–5472, doi:10.1002/2013GL058171.

Wollast, R. (1998), Evaluation and comparison of the global carbon cycle in the coastal zone and in the open ocean, in *The Sea, vol. 10*, edited by K. H. Brink and A. R. Robinson, chap. 9, pp. 213–252, John Wiley & Sons, N. Y.

Erratum

In the originally published version of this article, units where quantities were "per month" (mo^{-1}) were erroneously printed as "per mol" (mol^{-1}). The errors have been corrected, and this version may be considered the authoritative version of record.